ผลของการดัดแปรไทเทเนียมไดออกไซด์ด้วยโลหะทรานซิชัน (Y, La, Zr, Nb) ต่อการกระจายตัวของแพลตินัมและความว่องไวในปฏิกิริยาคาร์บอนมอนออกไซด์ออกซิเดชันของตัวเร่งปฏิกิริยา Pt/TiO_2

นายก้องกิตติ บุญกระโทก

วิทยานิพนธ์นี้เป็นส่วนหนึ่งของการศึกษาตามหลักสูตรปริญญาวิศวกรรมศาสตรมหาบัณฑิต
สาขาวิชาวิศวกรรมเคมี ภาควิชาวิศวกรรมเคมี
คณะวิศวกรรมศาสตร์ จุฬาลงกรณ์มหาวิทยาลัย
ปีการศึกษา 2558

EFFECT of TRANSITION METALS (Y, La, Zr, Nb) MODIFIED TiO_2 on Pt DISPERSION and C O OXIDATION ACTIVITY of Pt/TiO_2 CATALYST

Mr. Kongkitit Bungrathok

A Thesis Submitted in Partial Fulfillment of the Requirements
for the Degree of Master of Engineering Program in Chemical Engineering
Department of Chemical Engineering
Faculty of Engineering
Chulalongkorn University
Academic Year 2015

Thesis Title	EFFECT of TRANSITION METALS (Y, La, Zr, Nb) MODIFIED TiO_2 on Pt DISPERSION and CO OXIDATION ACTIVITY of Pt/TiO_2 CATALYST
By	Mr. Kongkitit Bungrathok
Field of Study	Chemical Engineering
Thesis Advisor	Associate Professor Joongjai Panpranot, Ph.D

Accepted by the Faculty of Engineering, Chulalongkorn University in Partial Fulfillment of the Requirements for the Master's Degree

.....Dean of the Faculty of Engineering

(Associate Professor Supot Teachavorasinskun, D.Eng.)

THESIS COMMITTEE

.....Chairman

(Professor Piyasan Praserthdam, D.Eng.)

.....Thesis Advisor

(Associate Professor Joongjai Panpranot, Ph.D)

.....Examiner

(Akawat Sirisuk, Ph.D.)

.....External Examiner

(Assistant Professor Okorn Mekasuwandumrong, D.Eng.)

ก้องกิตติ บุญกระโทก : ผลของการดัดแปรไทเทเนียมไดออกไซด์ด้วยโลหะทรานซิชัน (Y, La, Zr, Nb) ต่อการกระจายตัวของแพลตินัมและความว่องไวในปฏิกิริยาคาร์บอนมอนออกไซด์ออกซิเดชันของตัวเร่งปฏิกิริยา Pt/TiO_2 (EFFECT of TRANSITION METALS (Y, La, Zr, Nb) MODIFIED TiO_2 on Pt DISPERSION and CO OXIDATION ACTIVITY of Pt/TiO_2 CATALYST) อ.ที่ปรึกษาวิทยานิพนธ์หลัก: รศ. ดร. จูงใจ ปั้นประณต, 72 หน้า.

เตรียมตัวเร่งปฏิกิริยาแพลตินัมบนตัวรองรับไทเทเนียมไดออกไซด์ที่ดัดแปรด้วยโลหะทรานซิชัน (Y, La, Zr, Nb) โดยวิธีเคลือบฝังตามลำดับ ด้วยสัดส่วนโมล M/Ti ต่างๆ ในช่วง 0.001-0.1 เมื่อ M คือโลหะทรานซิชัน ตัวเร่งปฏิกิริยา $Pt/Y\text{-}TiO_2$ ที่มีสัดส่วน Y/Ti 0.001 แสดงตำแหน่งว่องไวจากการวัดด้วยการดูดซับของแก๊สคาร์บอนมอนออกไซด์มากกว่า Pt/TiO_2 ที่ไม่ผ่านการดัดแปร โดยที่ Y/Ti เท่ากับ 0.001 มีตำแหน่งว่องไวของ Pt ที่มากที่สุด และลดลงเมื่อเพิ่มสัดส่วน Y/Ti ตัวเร่งปฏิกิริยา $Pt/0.001Y\text{-}TiO_2$ แสดง light-off temperature ต่ำที่สุดที่ 85 องศาเซลเซียสสำหรับปฏิกิริยาคาร์บอนมอนออกไซด์ออกซิเดชัน ทั้งนี้ความว่องไวลดลงเมื่อเพิ่มสัดส่วน Y/Ti มากกว่า 0.001 อาจเนื่องมาจากแพลตินัมกระจายตัวบนยิตเทรีย ดังนั้นคาร์บอนมอนออกไซด์ที่ดูดซับบนแพลตินัมจึงไม่สามารถทำปฏิกิริยากับออกซิเจนในโครงสร้างของไทเทเนียมไดออกไซด์ได้ ผล ESR แสดง Ti^{3+} ในตัวอย่าง $Pt/0.001Y\text{-}TiO_2$ มีค่าสูงที่สุด และลดลงเมื่อเพิ่มสัดส่วนสารเติมแต่ง ซึ่ง Ti^{3+} มีส่วนช่วยเพิ่มการกระจายตัวและความว่องไวในปฏิกิริยา การกระจายตัวและความว่องไวของตัวเร่งปฏิกิริยา Pt/TiO_2 ที่ดัดแปรด้วยโลหะทรานซิชัน (Y, La, Zr, Nb) พบจำนวนตำแหน่งว่องไวและความว่องไวเพิ่มขึ้นสูงสุดที่ $Pt/0.005M\text{-}TiO_2$ และลดลงเมื่อเพิ่มสัดส่วน M/Ti ในแนวทางเดียวกับผลของ $Pt/Y\text{-}TiO_2$ ตัวเร่งปฏิกิริยาที่ถูกดัดแปรทุกตัวมีปริมาณ Ti^{3+} มากกว่า TiO_2 ซึ่งการเพิ่มขึ้นของ Ti^{3+} อาจมีความสัมพันธ์กับขนาดอะตอมหรือค่าอิเล็กโทรเนกาติวิตีของสารเติมแต่ง สรุปได้ว่าการดัดแปรตัวเร่งปฏิกิริยาแพลตินัมบนตัวรองรับไทเทเนียมด้วยโลหะทรานซิชันในช่วง 0.001-0.005 เป็นวิธีที่มีประสิทธิภาพในการเพิ่มการกระจายตัวของแพลตินัมและความว่องไวในปฏิกิริยาออกซิเดชันของคาร์บอนมอนออกไซด์

ภาควิชา วิศวกรรมเคมี ลายมือชื่อนิสิต .....

สาขาวิชา วิศวกรรมเคมี ลายมือชื่อ อ.ที่ปรึกษาหลัก .....

ปีการศึกษา 2558

5770378821 : MAJOR CHEMICAL ENGINEERING

KEYWORDS: CO OXIDATION / PLATINUM / TRANSITION METAL / TIO2 / DISPERSION / YTTRIA

KONGKITIT BUNGRATHOK: EFFECT of TRANSITION METALS (Y, La, Zr, Nb) MODIFIED TiO_2 on Pt DISPERSION and CO OXIDATION ACTIVITY of Pt/TiO_2 CATALYST. ADVISOR: ASSOC. PROF. JOONGJAI PANPRANOT, Ph.D, 72 pp.

Transition Metal (Y, La, Zr, Nb) modified TiO_2 supported Pt catalysts were prepared by successive impregnation with different M/Ti mole ratios in the range of 0.001-0.1, where M is the transition metal. The Pt/Y-TiO_2 with Y/Ti 0.001-0.05 showed higher active sites as measured by CO chemisorption than the unmodified Pt/TO_2. The highest Pt active sites were found at Y/Ti = 0.001 and declined as the Y/Ti ratio was further increased. The Pt/0.001Y-TiO_2 exhibited the lowest light-off temperature at 85°C for CO oxidation. The declined activity at higher Y/Ti mole ratio than 0.001 was probably due to Pt deposited on yttria. Thus, the CO adsorbed on Pt could not react with the oxygen in TiO_2 lattice. The ESR results showed the highest Ti^{3+} on Pt/0.001Y-TiO_2 and decreased when increasing dopant ratio. The presence of which Ti^{3+} promoted metal distribution and activity. The number of active sites and activity of the other transition metals (La, Zr, Nb) doped TiO_2 supported Pt catalysts were also increased with the Pt/0.005M-TiO_2 exhibited the highest values. Further increase of M/Ti ratios resulted in lower activity which was similar to the Pt/Y-TiO_2. For a dopant 0.005M-TiO_2 exhibited Ti^{3+} higher than TiO_2. The increasing of Ti^{3+} probably corresponded to atomic radius or electronegativity of dopant. In conclusion, doping the transition metals (Y, La, Zr, Nb) on the TiO_2 support in the range 0.001-0.005 mole ratio is an effective method to increase Pt dispersion on TiO_2 and CO oxidation activity of Pt/TiO_2.

Department:	Chemical Engineering	Student's Signature	.....
Field of Study:	Chemical Engineering	Advisor's Signature	.....
Academic Year:	2015		

ACKNOWLEDGEMENTS

I would like to express my sincere gratitude toward my advisor Assoc. Prof. Dr. Joongjai Panpranot and my co-advisor Professor Dr. Piyasan Praserthdam for the continuous support of my study and made my thesis completed. they guidance helped me throughout the duration of research and writing of this thesis.

I would like to thank Professor Dr. Piyasan Praserthdam as the chairman, Dr. Akawat Sirisuk, and Assistant Professor Dr. Okorn Mekasuwandumrong for, as the members of the thesis committee, for their comment and suggestion.

I gratefully thank The International Research Integration: Chula Research Scholar, Ratchadapiseksompot Endowment Fund for financial support.

CONTENTS

Page

THAI ABSTRACT iv

ENGLISH ABSTRACT v

ACKNOWLEDGEMENTS vi

CONTENTS vii

LIST OF FIGURES 10

LIST OF TABLES 12

CHAPTER I Introduction 13

1.1 Objective 15

1.2 The Scope of the research 15

1.3 Research methodology 17

CHAPTER II BACKGROUND 18

2.1 Titanium dioxide 18

2.1.1 Crystal structure and properties 18

2.1.2 Application of TiO_2 20

2.1.2.1 Pigment 20

2.1.2.2 Photocatalyst for waste treatment 21

2.1.2.3 Catalyst support 21

2.2 Modification of TiO_2 nanoparticles 21

2.3 Modified TiO_2 for supported noble metal catalysts 22

2.4 CO Oxidation 28

2.4.1 Langmuir-Hinshelwood mechanism 28

2.4.2 Eley-Rideal (ER) mechanism 29

Page

2.4.3 Mars-van Krevelen mechanism 29

2.4.4 Pt/TiO_2 in CO oxidation 30

CHAPTER III Experimental 34

3.1 Materials and chemicals 34

3.2 Preparation of catalyst 34

3.2.1 Preparation of modified TiO_2 supports 34

3.2.2 Preparation of Pt catalysts supported on modified-TiO_2 35

3.3 Catalyst characterization technique 35

3.3.1 CO-Pulse Chemisorption 35

3.3.2 N_2-physisorption 35

3.3.3 X-ray photoelectron spectroscopy (XPS) 36

3.3.4 Transmission electron microscopy (TEM) 36

3.3.5 H_2 temperature program reduction 36

3.3.6 X-ray Diffraction (XRD) 36

3.3.7 Electron spin resonance (ESR) 37

3.4 Catalyst activity on CO oxidation reaction 37

CHAPTER IV RESULTS AND DISCUSSION 40

4.1 The effect of yttria (Y/Ti malar ratio 0.001, 0.005, 0.01, 0.05, 0.1) modified TiO_2 on Pt active sites and CO oxidation activity of Pt/TiO_2 40

4.1.1 Effect of different dopant ratios on the properties of $Pt/Y\text{-}TiO_2$ 40

4.1.1.1 N_2 physisorption 40

4.1.1.2 X-ray Diffaction (XRD) 41

4.1.1.3 CO chemisorption 44

Page

4.1.1.4 H_2 temperature program reduction 45

4.1.1.5 X-ray photoelectron spectroscopy (XPS) 47

4.1.1.6 Electron spin resonance (ESR) 51

4.1.1.7 Transmission electron microscope (TEM) 52

4.1.2 Effect of different dopants on the activity of CO oxidation 56

4.2 The effect of different transition metal Y, La, Nb and Zr (M/Ti malar ratio 0.001, 0.005, 0.01, 0.05, 0.1) modified TiO_2 on Pt dispersion and CO oxidation activity of Pt/TiO_2 60

4.2.1 Effect of different dopant ratios on the properties of $Pt/M\text{-}TiO_2$ 60

4.2.1.1 CO chemisorption 60

4.2.1.2 XRD 61

4.2.1.2 H_2 temperature program reduction 62

4.2.1.4 XPS 62

4.2.1.5 Electron spin resonance (ESR) 63

4.2.1.6 Transmission electron microscope (TEM) 64

4.2.2 Effect of different dopants on the activity of CO oxidation 68

REFERENCES 72

APPENDIX 1

VITA 10

LIST OF FIGURES

Figure 2.1 Crystal structures of anatase (a), rutile (b), and brookite (c) [29] 19

Figure 2.2 Mars-van-Krevelen mechanism on Au/TiO_2 30

Figure 3.1 Flow diagram of the system for testing catalytic activity..... 39

Figure 4.1 N_2 adsorption-desorption isotherm of Pt/TiO_2 and $Pt/Y\text{-}TiO_2$ 41

Figure 4.2 XRD patterns of Pt/TiO_2 and $Pt/Y\text{-}TiO_2$..... 43

Figure 4.3 Effect of Y/Ti ratio on Pt active sites of the Pt/Y-TiO2 catalyst..... 44

Figure 4.4 H_2-TPR of $Pt/Y\text{-}TiO_2$ Catalysts 45

Figure 4.5 H_2-TPR of $Y\text{-}TiO_2$ support and $Pt/Y\text{-}TiO_2$ Catalysts with high Y/Ti ratios..... 46

Figure 4.6 XPS spectra of Ti 2p for Pt/TiO_2 and $Pt/Y\text{-}TiO_2$ 47

Figure 4.7 XPS spectra of Ti 2p for $Pt/0.05Y\text{-}TiO_2$ 48

Figure 4.8 XPS spectra of Y3d for $Pt/0.01\text{-}TiO_2$..... 49

Figure 4.9 XPS spectra of Y 3d for $Pt/Y\text{-}TiO_2$ with 0.01-0.1 Y/Ti mole ratios..... 50

Figure 4.10 XPS spectra of Pt4f for $Pt/0.01\text{-}TiO_2$..... 51

Figure 4.11 ESR spectra of $Pt/Y\text{-}TiO_2$ at 130K..... 52

Figure 4.12 TEM image of Pt/TiO_2 53

Figure 4.13 size distribution of Pt/TiO_2..... 53

Figure 4.14 TEM image of $Pt/0.001Y\text{-}TiO_2$ 54

Figure 4.15 size distribution of $Pt/0.001Y\text{-}TiO_2$ 54

Figure 4.16 TEM image of $Pt/0.1Y\text{-}TiO_2$..... 55

Figure 4.17 size distribution of $Pt/0.1Y\text{-}TiO_2$..... 55

Figure 4.18 TEM-EDX analysis of $Pt/0.1Y\text{-}TiO_2$..... 56

Figure 4.19 CO conversion over $Pt/Y\text{-}TiO_2$ and unmodified Pt/TiO_2 57

Figure 4.20 Turnover frequency (TOF) of Pt/Y-TiO_2 with different doped ratios 59

Figure 4.21 Effect of varies ratio of transition metals on Pt active sites..... 60

Figure 4.22 XRD pattern of Pt/0.005M-TiO_2..... 61

Figure 4.23 H_2-TPR of Pt/0.005Y-TiO_2 and Pt/0.005La-TiO_2 catalysts..... 62

Figure 4.24 XPS spectra of Ti 2p for Pt/TiO_2 and Pt/M-TiO_2..... 63

Figure 4.25 ESR spectra of Pt/0.005M-TiO_2 at 130K..... 64

Figure 4.26 TEM image of (a) Pt/0.005La-TiO_2 and (b) Pt/0.1La-TiO_2..... 65

Figure 4.27 TEM-EDX analysis of Pt/0.1La-TiO_2..... 65

Figure 4.28 TEM image of (a) Pt/0.005Nb-TiO_2 and (b) Pt/0.1Nb-TiO_2 66

Figure 4.29 TEM-EDX analysis of Pt/0.1Nb-TiO_2..... 66

Figure 4.30 TEM image of (a) Pt/0.005Zr-TiO_2 and (b) Pt/0.1Zr-TiO_2..... 67

Figure 4.31 TEM-EDX analysis of Pt/0.1Zr-TiO_2..... 67

Figure 4.32 CO conversion over 0.001M/Ti of transition metals modified Pt/TiO_2..... 68

Figure 4.33 CO conversion over 0.005M/Ti of transition metals modified Pt/TiO_2..... 69

Figure 4.34 CO conversion over 0.01M/Ti of transition metals modified Pt/TiO_2..... 69

LIST OF TABLES

Table 2.1 Some of the most important bulk properties of TiO_2 20

Table 2.2 noble metal supported modified TiO_2 26

Table 2.3 CO oxidation on Pt supported modified TiO_2 32

Table 3.1 Chemical used in catalyst preparation 34

Table 4.1 Physical properties of Pt/TiO_2 and $Pt/Y\text{-}TiO_2$ 41

Table 4.2 XRD analysis results of yttria modified TiO_2 supported Pt catalysts 43

Table 4.3 surface oxygen to lattice oxygen ratio by O 1s spectra 58

CHAPTER I

Introduction

Nowadays, noble metal catalysts are widely used in chemical industry and environment treatment reactions such as reforming, photocatalytic reaction, hydrogenation and oxidation [1-6]. Although, noble metal catalysts present high activity and selectivity but they are expensive. So, many researchers are now searching for low cost and high performance catalysts. The improvement of catalyst performance has been studied in terms of metal dispersion, preparation methods, addition of a second metal, and strong metal-supported interaction. Preparation of highly dispersed supported metal catalysts is necessary in order to gain high atomic efficiency of the noble metal.

Titanium dioxide (TiO_2) is commonly used as catalyst/catalyst support in photo-catalytic reaction, environment treatment, hydrogenation, and oxidation reaction because of its good chemical stability, non-toxic, and low cost [7]. Modification of support is recognized as a way to improve catalyst performance. The Pt supported on different types of TiO_2 supports exhibited different activity. TiO_2 crystallite size played role in the reducibility of the TiO_2 [8]. Mesoporous TiO_2 was found to exhibit higher photocatalystic activities than the Degussa P25 TiO_2 [9]. Transition metal doped TiO_2 led to structural properties change. Lanthanum doped TiO_2 resulted in inhibition of the growth of TiO_2 crystallite size [10, 11]. Khan and Cao [12] reported that Y^{3+} replaced lattice Ti^{4+} led to substitutional point defects in yttrium (Y)-doped TiO_2. It is also well known that TiO_2 is one of the reducible metal oxides which strongly interacts with noble metal [13, 14]. Strong metal support interaction (SMSI) effect is important for improving catalytic properties of supported metal catalysts in many reactions [15]. Many researchers reported the modification of supports for supported noble metal [7, 16, 17].

The addition of a second transition metal to supported noble metal catalysts has been reported to improve catalyst properties such as size, structure, metal composition, surface crystal structure, crystal defect, and metal particle size on supporting material [4, 18]. Tapina et al. [19] reported that addition of Re onto a Pd/TiO_2 monometallic catalysts, Re selectively deposited on $Pd\text{-}TiO_2$ interface by a catalytic reduction preparation method and random distribution obtained by successive impregnation. Yttria-doped Pt/TiO_2 ($Pt/TiO_2–YO_x$) prepared by sol-gel method was found to efficiently improve the activity and stability as well as maintain the naturally excellent sulfur resistance in diesel oxidation and showed ultrafine platinum nanoparticles (<1 nm) on $TiO_2–YO_x$ supports [20]. Yttria is known to be for its superior inertness to chemical attack from molten Ti alloy [21]. Addition of Mo and Fe was reported to the result in the formation of a low valent thin oxide layer over TiO_2 surface and Pt metal were highly dispersed on the layer [22].

Pt/TiO_2 catalyst is used in many catalytic reactions. For examples, 0.3 wt% $Pt\text{-}TiO_2$ was used in the selective hydrogenation of 3-nitroacetophenone. High activity and excellent selectivity were attributed to Pt nanoparticles and TiO_2 support as well as the interaction between them [23]. Pt/TiO_2 exhibited higher photocatalytic activity than TiO_2 particles [24]. For cyclohexane photocatalytic oxidation on Pt/TiO_2 catalysts, the conversion was found to decrease by increasing Pt loading but CO_2 selectivity was higher than TiO_2 [25].

The carbon monoxide (CO) oxidation reaction is an important reaction in environment pollution control. This reaction is known to be less structure sensitive or structure insensitive which the activity depends on the amount of active sites. The improvement of metal dispersion consequentially affects CO oxidation activity. The surface properties of support metal were used to describe the catalytic activities of metal dispersed on support. Thus, CO oxidation is a good model reaction to gain more understanding of the modified catalyst. Li et al. [5] reported that particle size of Pt is related to turnover efficiency of CO oxidation.

In the present work, the first parts, a commercially available P-25 TiO_2 was modified by Y, Zr, Nb, and La and used as catalyst support for preparation of Pt/TiO_2

catalysts. The catalyst activity was evaluated in the CO oxidation reaction and characterized by various analytical techniques.

1.1 Objective

To investigate the effect of transition metals (Y, Zr, Nb, La) modified TiO_2 on Pt active sites and CO oxidation activity on Pt/TiO_2 catalysts.

1.2 The Scope of the research

The scope of the research is given below.

1.2.1 Modified TiO_2 were prepared by successive impregnation. Transition metal (Y, Zr, Nb, La) was loaded on the TiO_2 (P25) first and followed by platinum loading.

1.2.2 TiO_2 support was modified with different mole ratios of transition metals/Ti (0.001, 0.005, 0.01, 0.05, 0.1) mole ratio and loaded with 0.3wt% Pt.

1.2.3 The catalyst activity testing was carried out in the CO oxidation reaction. The feed containing 1%CO and 2%O_2 balance with He was flowed through reactor at 50 ml/min with heating rate 2°C/min.

1.2.4 Characterization of catalyst by using various techniques:

- X-ray diffraction (XRD)
- N_2 physisorption
- CO chemisorptions
- H_2 Temperature program reduction (H_2 TPR)
- X-ray photoelectron spectroscopy (XPS)
- Transmission electron microscope (TEM)
- Electron spin resonance (ESR)

1.3 Research methodology

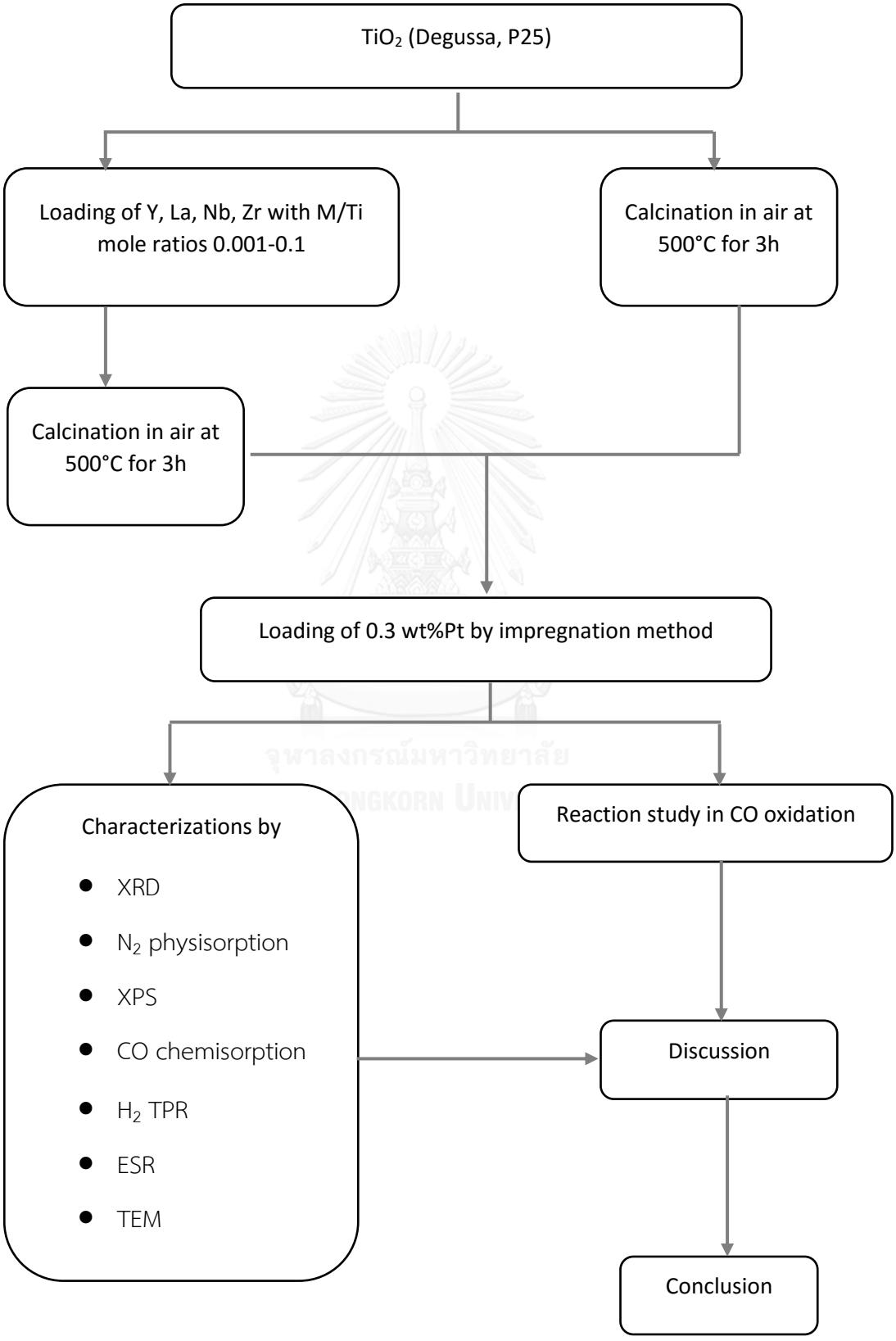

CHAPTER II
BACKGROUND

This purpose of this chapter provides the fundamental concept and literature review for this thesis. The first section of the chapter describes the fundamental information about properties of TiO_2, applications and surface modification. Next section describes transition metal modified TiO_2 supports. The fundamental of CO oxidation was mentioned in the last section.

2.1 Titanium dioxide

TiO_2 so celled titania, has many applications due to its strong oxidizing power of the photogenerated holds, chemical inertness, non-toxicity, low cost, high refractive index and other advantageous surface properties. Therefore, TiO_2 was used as catalyst or catalyst support such as photocatalysis, air purification, water treatment, self-cleaning, antifogging, gas sensors, and other [26-28].

2.1.1 Crystal structure and properties

Titanium dioxide has three crystal forms: anatase (tetragonal), rutile (tetragonal) and brookite (orthorhombic), the structure are illustrated in **Figure 2.1** Crystal structures of anatase (a), rutile (b), and brookite (c). The rutile and anatase structure with tetragonal geometry are highly symmetrical where each Ti atom is surrounded by six oxygen atom forming a TiO_6 octahedron**.** The only difference between the two structures is the distortion and linkage between the octahedrally coordinated Ti and O atoms [29]. Rutile is common form and the most stable form of TiO_2. Anatase and brookite convert to rutile at high temperature. Anatase and rutile have been widely studies and used in many applications due to brookite is uncommon and difficult to purify.

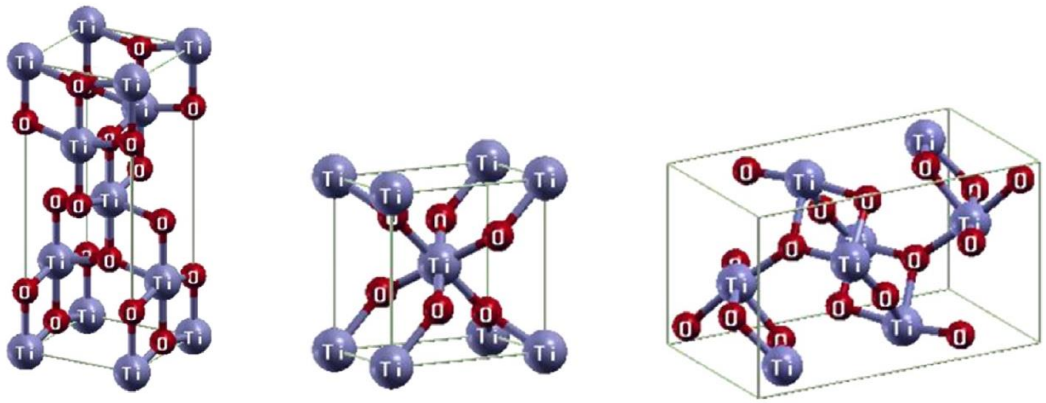

Figure 2.1 Crystal structures of anatase (a), rutile (b), and brookite (c) [29]

Titanium dioxide is sensitive to thermochemical such as temperature, pressure, impurity. TiO_2 surface contains several atoms, ions and molecules via ionic, covalent or coordinated bonding such as basic terminal and acidic bridged-hydroxyl group; unstable Ti-O-Ti bonds; water molecules adsorbed at Lewis acid sites or bound to surface hydroxyl group; potential electron donor and acceptor sites; perhaps adsorbed oxidants such as hydroxyl or hydroperoxyl radicals; or activated oxygen species generated by photocatalytic processes [30]. The crystal planes (1 0 0), (0 0 1) and (1 1 0) are found in Rutile phase, where (1 1 0) is most stable. The crystal planes of anatase are found in (1 0 1), (1 0 0) and (0 1 0). There TiO_2 crystal planes plays role in all mentioned applications. Some of the most important bulk properties of TiO_2 are shown in **Table 2.1** Some of the most important bulk properties of TiO2. The structure defects is the main factor affecting the properties of crystalline of material. Oxygen vacancies (Ti^{3+}) is dominant surface defect on TiO_2 which easily detected by XPS, O_2 photodesorption, surface vertical orbital (SVO) method, electron spin resonance (ESR) or CO_2-temperature programmed desorption (TPD) [31]. It plays a critical role in surface and electronic properties of TiO_2 and is believed to affect the electron–hole recombination process in photocatalysts [32]. Linh et al. [33] performed density functional theory (DFT) based calculations to investigate the effects of O-vacancies on the adsorption of O_2 on anatase TiO_2 (001). The O_2 adsorption on TiO_2 (001) was enhanced by introducing O-vacancy. The resulting excess electrons from the

introduction of the O-vacancy redistribute around the neighboring Ti ions. An incoming O_2 can adsorb at the O-vacancy site, either in the superoxide state (O_2^-) or the peroxide state ($O2_2^{2-}$). Bailón-García et al. [3] reported that after Pt/TiO_2 pretreated in H_2, the formation of two-dimensional Pt nanoparticles and oxygen vacancies favored the diffusion of Pt species into the TiO_2 structure. The coupled effect of Pt 2-D nanoparticles and oxygen vacancies strongly enhanced the catalytic activity and the selective hydrogenation of citral.

Table 2.1 Some of the most important bulk properties of TiO_2

Crystal structure	system	Lattice parameters			Band gap (eV)
		a	b	c	
Rutile [34]	Tetragonal	4.592	-	2.958	3.00 [35]
Anatase [36]	Tetragonal	3.785	-	9.511	3.21 [35]
Brookite [37]	Orthorhombic	9.184	5.447	5.145	3.13 [35]

Degussa P25, TiO_2 is titania nanoparticles that is used widely because of excellent activity in many photocatalytic reaction systems. It is known that P25 contains anatase and rutile phase in ratio 70:30 and large surface area (49 m^2 g^{-1}) [38, 39].

2.1.2 Application of TiO_2

TiO_2 is consumed in many applications such as pigment, photocatalyst, catalyst supported, promoter, gas sensor, or containing in sunscreen and so on.

2.1.2.1 Pigment

Titanium dioxide is the most widely used white pigment in a variety of industrial products, such as plastics, printed products and paints. Moreover, thermal property of

TiO_2 is used in household paints which reducing the energy required for cooling [40]. And UV resistant property is used in cosmetic product such as sun screen.

2.1.2.2 Photocatalyst for waste treatment

An expanding Industry causes lots of waste which requires disposal treatment and costly. Semiconductor photocatalysis has been considered to solving the environmental problem. Many researchers have propose that TiO_2 is excellent photocatalsyt, it is low toxicity, low-cost and high efficiency to degradation of organic pollutants in atmosphere and water [41-44].

2.1.2.3 Catalyst support

Titanium dioxide (TiO_2) is commonly used as catalyst/catalyst support because of low-cost and large surface area. Because of its good chemical stability, non-toxic, and low cost [7]. And it is well known that TiO_2 is one reducible metal oxides which strong interacts with noble metal [13, 14]. Strong metal support interaction (SMSI) effect is important for improving catalytic properties of supported metal catalysts in many reaction [15].

2.2 Modification of TiO_2 nanoparticles

The properties of TiO2 nanoparticles depend on morphology, size, crystalline phase, and electron properties.

Preparation of TiO2 nanostructure with significant properties have been developed in many processes. Many researchers were interested in precipitation, sol-gel, hydrothermal, and flame spray preparation method [45-48]. Among the above mentioned methods, the sol-gel method is normally used for preparation of nanometer sized TiO_2 powder with different shapes such as porous structure, thin fibers, dense powder, and thin films, as well as for the surface treatment of metal oxides. There are several parameter for controlling sol-gel process to prepare TiO_2

nanopowder with significant properties, such as mole ration of reactant, water content, temperature, time, and pH of the media [49, 50]. The TiO_2 prepared by sol-gel method usually present an amorphous structure which must be heat-treated in order to achieve the crystalline phase [51]. The different morphological characteristics of a TiO_2 is played role on TiO_2 properties which affect to catalystic activity or behavior with metal loading [8].

Addition of a second element is a technique used to improve the TiO_2 properties. Two main techniques have been reported. The first one is the incorporation of second element into TiO_2 lattice by sol-gel, co-precipitation and hydrothermal. For another one technique, the second component is placed on TiO_2 surface by impregnation method which is easy method to prepare lot of catalyst. Wang et al [52] observed that Nb promotes the anatase to rutile phase transition but has a depression effect on the anatase grain growth in Nb-doped TiO_2 prepared by sol-gel method. Khan and Cao [12] reported that yttrium (Y)-doped TiO_2 prepared by hydrothermal method, Y^{3+} replaces lattice Ti^{4+} leading to substitutional point defects. The incorporation of yttrium into the titania lattice create oxygen vacancies which the quantity of dopant controls the number of surface oxygen vacancies created and the gold particle size. The oxygen vacancies generated to balance the charge (bridge surface oxygen atoms) are found to be preferential adsorption sites for Au atoms and NPs, acting as nucleation centers that favor the dispersion of catalyst active phase on support surface [53]. Lanthanum doped 1D-TiO_2 nanomaterials prepared by wet impregnation method was reported. La was found to inhibits TiO_2 crystallite growth and increase the lifetime of photogenerated electron–hole pairs in photodegradation reaction [11].

2.3 Modified TiO_2 for supported noble metal catalysts

Previous works of noble metal supported modified TiO_2 is presented in **Table 2.2.**

T. Sakamoto, et al. (2010) investigated the addition effect of transition metals (Fe, Ni, Sn, Co, Mo, Ru) modified TiO_2 supported Pt metal by successive impregnation method for liquid phase reforming of methanol. They reported that additive Mo, Fe

increased catalytic activity and selectivity of Pt/TiO_2 remarkably. The dispersion of metal increased from 13.6% to 29.9% and 39.9%, respectively. The Mo and Fe species formed a low valent thin oxide layer over TiO_2 surface and then Pt metal were highly dispersed on that layer. However, additive Ni or Co formed alloy with Pt which exhibited poor improvement activity and selectivity [22].

B. Tapin, et al. (2014) prepared Bimetallic Re-Pd catalysts by addition of Re onto Pd/TiO_2 monometallic catalyst, either by a catalytic reduction method or by successive impregnation. They reported that catalytic reduction preparation method induced a selective Re deposit at the Pd–TiO2 interface but successive impregnation method lead to random distribution [19].

Z. ma, et al. (2007) prepared $Au/M_xO_y/TiO_2$ for CO oxidation. The metal oxide-modified TiO_2 were prepared by excess-solution impregnation method and gold was loaded by a deposition-precipitation method. They found that Au/TiO_2 modified by CaO, NiO, ZnO, Ga_2O_3, Y_2O_3, ZrO_2, La_2O_3, Pr_2O_3, Nd_2O_3, Sm_2O_3, Eu_2O_3, Gd_2O_3, DY_2O_3, Ho_2O_3, Er_2O_3, or Yb_2O_3 could improve activity even after aging at 500°C in O_2-He. Moreover, catalyst showed high activity even at -100°C when it was calcined at 200°C [54].

Y. Sato, et al. (2005) studied Addition effect of Re on the water gas shift reaction over TiO2 supported Pt, Pd and Ir catalysts. Addition Re were observed that possible formation of bimetallic surface clusters with Re in the cases of Pt and Pd and anchoring of nanoparticles by highly dispersed Re over TiO_2 in the case of Ir [55].

Z. Yang, et al. reported that Yttria-doped Pt/TiO_2 was found to remarkably improve the activity and stability as well as maintain the naturally excellent sulfur resistance of TiO_2-based catalysts in diesel oxidation. The yttria-doped TiO_2 was prepared by co-precipitation and Pt was loaded to support by impregnation methods. Tem image of Pt/TiO_2-YO_x show that ultrafine platinum nanoparticles (<1 nm) with a narrow size distribution (0.31–1.29 nm) were dispersed on TiO_2–YO_x supports. The XRD patterns confirm that yttria addition could lead to suppression of the anatase crystal growth and phase transition which could consequently enhance the platinum

dispersion. They conclude that yttria can act as a dispersion promoter and a structure stabilizer which is beneficial to low-temperature diesel oxidation catalytic activity and stability [20].

J. Plata, et al. studied yttrium modified TiO_2 supported gold. The support was prepared by sol-gel method. I was found that yttrium incorporated into titania lattice favors the formation of oxygen vacancies while at low Y loadings the anatase structure is preserved. The CO oxidation actives is known to be significantly dependent on amount of dopant controls the number of surface oxygen vacancies created and gold particle size. Density functional theory based calculations show that Y atoms are incorporated at the TiO_2 surface at substitutional positions only, while the preferred oxygen vacancies arise by removing the bridge surface oxygen atoms. These O-vacancies are the preferential adsorption sites for Au atoms and nanoparticles, acting as nucleation centers that favor the dispersion of the catalyst active phase over the support surface [53].

D. Clark, et al. developed a catalyst for CO oxidation which is effective in the presence of SO_2 and water in Claus tail gas. The catalyst were prepared by two case, first Au and La_2O_3 were deposited on TiO_2 nano-materials and the second, Au was deposited on a co-precipitated TiO_2–La_2O_3 nano-material. Both catalyst showed vary high CO conversion above 323K and remained active in the presence of SO_2 and other sulfur compounds. The very high catalytic activity of the co-precipitated catalyst was attributed to the presence of cationic Au and a low level of sulfate formation on the nano-fiber support [56].

Hou, et al. prepared mesoporous TiO_2 and La-TiO_2 supported gold catalyst by using deposit-precipitation method. The gold in Au/TiO_2 calcined at 450°C present as AuO but La^{3+} doped Au/TiO_2 present a small portion of Au_2O_3 in addition to AuO. The HRTEM image show that the crystallite sizes of Au in Au/TiO_2 and Au/La-TiO_2 after calcination at 400°C are 6~8 nm and ~5 nm, respectively. After calcination at 450°C, the crystallite sizes of Au in Au/TiO_2 increase above 20 nm but La doped Au/TiO_2 still small size ~9nm. After calcination at 450°C, completely conversion of CO over Au/TiO_2 reaches 86°C, while the temperature is only 53°C over Au/La-TiO_2. indicating that small

amount La^{3+} doped Au TiO_2 effectively inhibits the sintering of Au crystallites and makes the catalyst possess good activity and high thermal stability [57].

A. Luengnaruemitchai, et al. (2015) prepared a series of Au supported on Fe_2O_3-TiO_2 catalysts for the preferential CO oxidation (PROX) under a H_2-rich stream. The effects of the different metal support ratio, the calcination temperature, the gold loading, and the pre-treatment condition were studied. They report that 1% Au/Fe_2O_3-TiO_2 (1:4) exhibited higher CO conversion than the 1% Au/TiO_2 and 1% Au/Fe_2O_3 catalysts, especially temperature lower than 100°C, which due to the formation of reducible gold species at lower temperature. TPR results explain that the improvement of Au-Au and metal-metal (in support) interaction. XPS spectra exhibit peaks of Au^0 which assigned to active site. The O_2 pretreatment could form adsorbed oxygen species no surface which exhibit negative effect on activity and selectivity [58].

N.R. Elezovic, et al. (2011) studied Nb–TiO_2 supported platinum nanocatalyst for oxygen reduction reaction in alkaline solutions. 5% Nb doped TiO_2 was synthesized by modified acid-catalyzed sol–gel procedure in non-aqueous medium. Only anatase phase was found by XRD. Existence of any peaks belonging to Nb compounds has not been observed, indicating Nb incorporated into the lattice. Pt was loaded to Nb-TiO_2 by using borohydride reduction method. 4nm of Platinum distribution over Nb doped TiO_2 support was quite homogenous [59].

All literature suggested that transition metal could modify TiO_2 support properties such as inhibit phase transform and substitution into titania lattices which create defect on support surface. Moreover, it could improve metal properties such as increase metals dispersion, reduce metal size and change metal-support interaction which lead to increasing catalytic activity.

Table 2.2 noble metal supported modified TiO_2

Catalyst	Main catalyst	Additive metal	Preparation	Reaction	Detail	Ref.
Pt/M-TiO_2	5wt%	5wt.% Fe, Ni, Sn, Co, Mo, Ru	Successive impregnation	Liquid phase reforming of methanol	Pt were highly dispersed on the Fe, Mo layer	[22]
Re-Pd/TiO_2	2.0wt% Pd	0.9-3.5wt.% Re	1. successive impregnation, 2. catalytic reduction	selective hydrogea-tion of succinic acid in aqueous phase	SI: Re is random distribution CR: Re deposit at the Pd–TiO_2 interface	[19]
Au/M_xO_y/TiO_2	n/a	5wt.% M_xO_y (M: Ca, Ni, Zn, Ga, Y, Zr, and Si-W)	impregnation	CO oxidation	metal oxide additives decrease Au size	[54]
Pt-Re/TiO_2	2wt.% Pt	1-10wt.% Re	Successive impregnation	water gas shift	Increasing of dispersion and particle sizes	[55]
Pt/TiO_2-YO_x	1wt.% Pt	27wt.% Y	co-precipitation and incipient impregnation	diesel oxidation catalysts	Ultrafine Pt nanoparticl es (<1nm)	[20]

Au/Y-TiO_2	n/a	n/a	sol–gel and deposition–precipitation	CO-oxidation	incorporated Y atom at TiO_2 surface are create vacancy sites, which adsorption sites for Au	[53]
Au–La_2O_3–TiO_2	1wt.% Au	n/a	co-deposited	CO oxidation	La^{3+} cation has been incorporated into TiO_2 matrix during the co-precipitation process	[56]
Au/La-TiO_2	n/a	n/a	deposit-precipitation	CO oxidation	The doping of a small amount of La^{3+} effectively inhibits the sintering of Au crystallites	[57]
Au/Fe_2O_3-TiO_2	1wt.% Au	17.wt.% Fe	incipient-wetness impregnation	CO oxidation	Improve-ment of Au-Au and metal-metal	[58]

					(in support) interaction in TPR	
Pt/Nb-TiO_2	20wt.% Pt	5wt.% Nb	Sol-gel and borohydride reduction	Oxygen reduction	4nm Pt particle	[59]

2.4 CO Oxidation

Carbon monoxide is a colorless, odorless and poisonous gas which is a major product of the incomplete combustion of hydrocarbon. It is a byproduct of vehicle exhausts, which a very large amount of CO emission in cities, particularly in heavy traffic area. Other large CO emission source include industrial process, boiler and incinerator. The emission of CO is a dangerous pollutant that is admitted contribute to greenhouse effect and global warming. The carbon monoxide is very dangerous to human due to colorless and odorless, which can despoil oxygen-carrying in hemoglobin by inhaling and lead to hypoxic injury, neurological damage, and possibly death. Due to CO oxidation is structure insensitive, it was used as reaction for studying influence of modified catalyst.

2.4.1 Langmuir-Hinshelwood mechanism

It is generally admitted that CO oxidation on transition metal followed a Langmuir-Hinshelwood mechanism. The carbon monoxide and oxygen molecules can adsorb on transition metal and take place at metal dispersed catalysts. The mechanism have been proposed during the CO oxidation [60]:

1) CO is adsorbed on surface of metal catalysts;

$$CO_{(g)} + * \longleftrightarrow CO_{(ad)} \quad (2.1)$$

2) Oxygen is adsorbed on surface of metal catalysts;

$$O_{2\,(g)} + * \longrightarrow O_{2\,(ad)} \quad (2.2)$$

3) Oxygen on surface is dissociated to form oxygen adatoms;

$$O_{2\,(g)} + * \longrightarrow 2O_{(ad)} \quad (2.3)$$

4) Adsorbed CO molecule reacted with adsorbed oxygen to form CO_2

$$CO_{(ad)} + O_{(ad)} \longrightarrow CO_{2\,(ad)} + * \quad (2.4)$$

5) Adsorbed CO_2 is desorbed from active site

$$CO_{(ad)} + \longleftrightarrow CO_{2\,(g)} + * \quad (2.5)$$

Where * is a vacant active site

2.4.2 Eley-Rideal (ER) mechanism

Eley–Rideal-type (ER-type) mechanisms involve the reaction of adsorbed CO with molecular O_2 in the gas phase which reactant in gas phase react with adsorbed reactant. According to the two-step mechanism, first O_2 does not adsorb on catalyst surface but is react from the gas phase by CO adsorbed on Au, and forms the reaction intermediate (COOO) either on the Au surface. This reaction intermediate then decomposes into CO_2 leaving an adsorbed O atom on the Au surface. In the second step, this remaining O atom reacts with another CO molecule adsorbed on Au, leading to the formation of the second CO_2 molecule [61, 62], which shown in equation 2.6-2.7.

$$O_{2\,(g)} + CO_{(ad)} \rightarrow CO_{2\,(g)} + O_{(ad)} \quad (2.6)$$

$$CO_{(g)} + O_{(ad)} \rightarrow CO_{2\,(g)} + * \quad (2.7)$$

2.4.3 Mars-van Krevelen mechanism

Mars-van Krevelen mechanism is participation of lattice O atom in CO oxidation reaction which has been proposed to explain the CO_2 and CO_3^{2-} formation upon metal oxide exposure to CO. In this case, the oxygen atoms on the surface must be reactive enough to allow the adsorption of CO at these sites. Such sites do not exist on perfect

stoichiometric surfaces and require some corrugation. Once CO has adsorbed on metal site and approached the activated O atom, an electron transfer takes place from the molecule to the surface and the cationic sites are reduced. As a result, CO binds to one surface O forming CO_2, or to two surface O forming carbonates CO_3^{2-}, at the same time that titanium cations are reduced [63].

The Mars-van Krevelen mechanism on Au/TiO_2 is shown in Figure 2.2. The CO adsorbed on Au nanoparticle then reacted with activated surface lattice oxygen species at the perimeter of the $Au\text{-}TiO_2$ interface and CO_2 product desorbed to gas phase. Oxygen lattice site was replenished by dissociative adsorption of O_2 at them. At higher temperatures (>80°C), migration of surface lattice oxygen and surface oxygen vacancies also gives access to neighboring oxygen surface lattice sites [64].

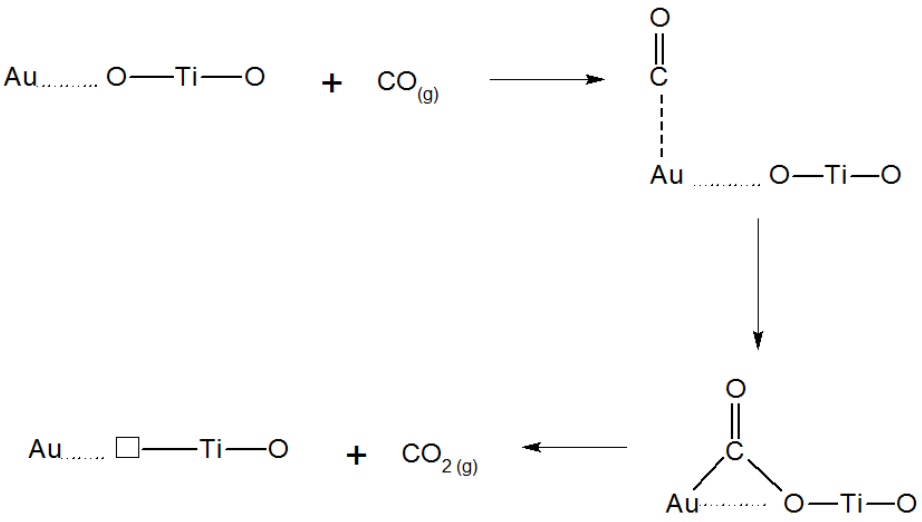

Figure 2.2 Mars-van-Krevelen mechanism on Au/TiO_2

2.4.4 Pt/TiO_2 in CO oxidation

Previous works of CO oxidation on Pt supported modified TiO_2 is presented in Table 2.3.

N. Li, et al. studied kinetic and the effect of particle size on low temperature CO oxidation over Pt/TiO_2 catalysts. Pt/TiO_2 catalysts with various Pt particle sizes prepared by using an incipient wetness method. They report that turnover frequencies

of CO oxidation depend on Pt dispersion which declined when increasing Pt particle size. However, turnover frequency based on Pt atoms located on the periphery of Pt–TiO_2 interface remained constant at 40°C, implying that these periphery Pt atoms were the active sites. The elementary steps of this reaction were proposed that CO adsorbed on Pt atom and O_2 adsorbed on TiO_2 and then a reaction of these two species at the Pt-TiO_2 interface [5].

Hisahiro Einaga, et al. (2014) studied effect of varied molar ratio of Fe to Pt from 0.2 to 1.0 on Pt-Fe/TiO_2 catalyst with 1 wt% Pt. The TiO_2 support Pt-Fe catalysts were prepared by impregnation method from acetylacetonate complexes. The preparation route for TiO_2-supported Pt and Fe were found to affect to CO chemisorption and catalystic activity. Co-impregnation catalyst Pt-Fe/TiO_2 exhibits the highest activity, indicating that the close proximity of Pt and Fe is crucial to obtaining the improved activity of CO oxidation. HAADF-STM image of the 1 wt% Pt-Fe/TiO_2 catalyst with the Fe/Pt ratio of 1.5 showed the 20-30 nm particles size of TiO_2 and 2 nm of Pt particles distributed over the TiO_2 surface. Fe oxide particles were not observed in TEM image and not detected in the XRD patterns of Pt-Fe/TiO_2, indicating that Fe species were highly dispersed on TiO_2 surface. The temperature programed reduction profile of Pt-Fe/TiO_2 with the Pt loading 10% and the Fe/Pt ratio of 1/5 not observed reduction peak of Fe^{3+} to Fe^{2+} and Fe^{2+} to metallic Fe^0 at 200-350°C and 530-850°C respectively, compare to FeO_x/TiO_2 with 5 times larger. On the other hand, Pt–Fe/TiO2 catalyst showed much different TPR profile. A negative peak at 64°C was assigned to H_2 desorption from Pt particles. The broadening peaks in the temperature range of 200–770°C were ascribed to reduction of oxidized Fe species and subsequent formation of metallic Fe species. Thus, the H_2 reduction of oxidized Fe species was promoted by Pt [4].

Ken-Ichi Tanaka, et al. (2006) reported that CO oxidation on FeO_x/Pt/TiO_2 catalyst is improved by H_2 and/or H_2O at 60°C. DRIFT-IR spectroscopy shows that fraction of bridge bonded CO increases while that of linearly bonded CO decreases on the FeO_x loaded Pt/TiO_2 catalyst. The bridged CO is more reactive than the linearly bonded CO with respect to O_2 [65].

Hongmei Qin, et al. (2015) studied $Pt/MO_x/TiO_2$ where M are Al, Fe, Co, Cu, Zn, Ba, La. The commercial TiO_2 were loaded additive and Pt by conventional impregnation. It was observed that all of the additives promote catalytic activity of CO oxidation. XRD not detect peaks of addition metals [66].

P. Won Seo, et al. (2010) studied a characteristics of CO oxidation at room temperature by metallic Pt. The 1 wt% platinum was loaded to commercial TiO_2. Pt/TiO_2 catalyst can increase the oxidizing capability of CO at low temperature and room temperature by reduction. They found that the reduced catalyst changed the platinum's oxidation value to Pt^{+2} and Pt^{+0}. The catalyst consists of non-stoichiometic platinum oxidized species showed excellent ability to accept oxygen which exhibit high CO conversion at low temperature and room temperature [67].

R. Green, et al. (2004) studied CO TPD on 2.5 wt% Pt/TiO_2. They surprising observed that CO_2 is adesorption produce, even though oxygen is not dosed into the system. The repeated experiments result in the same amount of CO_2 desorption. It is possible explanation might be that CO adsorbed on Pt site and spillover to TiO_2 support producing CO_2 by react to oxygen in TiO_2 lattice. Ti^{3+} creating by removed oxygen is diffuse into bulk of TiO_2 crystallite which effectively removes the surface non-stoichiometry [68].

Table 2.3 CO oxidation on Pt supported modified TiO_2

Catalyst	Pt	additive metal	Preparation methods	Detail	Ref.
Pt/TiO_2	2 wt.%		incipient wetness impregnation	TOFs based on Pt dispersion varied as declined with increasing Pt particle size	[5]
$Pt\text{-}Fe/TiO_2$	1wt%	0.2-1.0wt% Fe	Co-impregnation	$Pt\text{-}Fe/TiO_2$ higher activity	[4]

				TEM : 2nm Pt and Fe oxides were not observed	
$FeO_x/Pt/TiO_2$	1wt% Pt	n/a	dipping	bridge bonded CO increases while linearly bonded CO decreases	[65]
$Pt/MO_x/TiO_2$	n/a	Al, Fe, Co, Cu, Zn, Ba, La	conventional impregnation	addition metals promote CO oxidation	[66]
Pt/TiO_2	1wt%			The catalyst consists of non-stoichiometic platinum oxidized species showed excellent ability to accept oxygen which exhibit high CO conversion at low temperature and room temperature	[67]
Pt/TiO_2	2.5wt%		incipient wetness impregnation	CO_2 is a desorption produce from CO TPD	[68]

CHAPTER III

Experimental

3.1 Materials and chemicals

The chemicals used in catalyst preparation are listed in Table 3.1.

Table 3.1 Chemical used in catalyst preparation

Chemicals	Chemicals name	Purity (%)	Suppliers
$H_2PtCl_6 \cdot xH_2O$	Chloroplatinic acid hydrate	99.9	Aldrich
$C_{12}H_{28}O_4Zr$	Zirconium (IV) propoxide	70	Aldrich
$LaN_3O_9{\cdot}6H_2O$	Lanthanum nitrate hexahydrate	99	Himedia
$Y(NO_3)_3{\cdot}6H_2O$	Yttrium (III) nitrate hexahydrate	99.9	Aldrich
$C_4H_4NNbO_9{\cdot}xH_2O$	Ammonium niobate(V) oxalate hydrate	99.9	Aldrich

3.2 Preparation of catalyst

The details of the preparation method for modified TiO_2 supported Pt catalysts are present as follows:

3.2.1 Preparation of modified TiO_2 supports

The modified TiO_2 supports were prepared by dry impregnation methods. 2g of titania was doped with aqueous solution containing transition metal percursor (dopant/Ti molar ratios = 0.001, 0.005, 0.01, 0.05, 0.1). The solution was slowly dropped onto titania support to obtain the desired ratio (calculation was show in appendix A.1) and dried in oven 110°C overnight before calcined in calcined tube at heating rate 10°C/min and held for 500°C for 3h with air flow. The modified TiO_2 support was obtained.

3.2.2 Preparation of Pt catalysts supported on modified-TiO_2

Supported metal catalysts were prepared by successive dry impregnation method using 0.3 wt% Pt (Chloroplatinic acid hydrate from Aldrich) aqueous solution. The aqueous solution of Pt precursor was slowly dropped on transition modified TiO_2 support to obtain the desired mole ratio of catalyst (calculation as shown in appendix A.2). After impregnation, the catalyst were dried in oven at 100°C overnight and then calcined in air 500°C for 3h. The obtained catalyst were noted as Pt/0.001Y-TiO_2 (Pt/ transition mole ratio–TiO_2).

3.3 Catalyst characterization technique

The characterization technique were used to gain more understanding of catalyst structure and texture properties.

3.3.1 CO-Pulse Chemisorption

The active sites of platinum catalyst was determined by CO-Pulse chemisorption technique using Micromeritics ChemiSorb 2750 and ASAP 2101C V.3.00 software. 50mg of catalysts was reduced in Hydrogen at 500°C for 1h. Then simple was heated up to 510°C in Helium flow for 10min and cool down to room temperature. After that, CO pulses were injected until the quantity of CO pulse reached a steady. CO chemisorbed Calculation was shown in appendix B.

3.3.2 N_2-physisorption

The surface area, pore volume and pore diameter were measured by low temperature nitrogen technique using Micromeritics ChemSorb 2750 Pulse chemisorption system. Calculations were performed on the basis of the BET isotherm. Before the experiment, the simples were pretreat at 110°C for 3h.

3.3.3 X-ray photoelectron spectroscopy (XPS)

XPS was used to investigate the binding energy and surface composition of catalysts by using an Amicus photoelectron spectrometer with Mg K_α X-ray source at current of 20 mA and 10eKV. The binding energy was calibrated by the C 1s peak at 285.0 eV. The computer controlled by using the AMICUS "VISION2" software.

3.3.4 Transmission electron microscopy (TEM)

The morphology and size of metal catalysts were investigated by JEOL model JEM-2100 (200kV) transmission electron microscopy using energy-dispersive X-ray detector operated at 80-200kV. Prior to analysis, The sample was dispersed in 2 ml of ethanol using ultrasonic vibration then the solution was dropped on copper gird coated polymer, following to dry in atmospheric air and then kept in desiccator.

3.3.5 H_2 temperature program reduction

The reduction behaviors of samples were measured by hydrogen temperature-programmed reduction (H_2-TPR) experiments. The samples were placed in a quartz reactor, and then heated from room temperature to 800°C at a rate 10°C min^{-1} in 10% H_2 in Ar. The hydrogen consumption was determined by thermal conductivity detector (TCD). The water produced in TPR was trapped by a cold trap.

3.3.6 X-ray Diffraction (XRD)

The X-ray diffraction (XRD) patterns were analyzed by X- ray diffractometer (Bruker D8 Advance) using Cu K_α irradiation at range between 20° and 80° with a step of 0.05° s^{-1}. The lattice parameter and d-spacing were calculated based on Bragg's law. Crystallite size was calculated by Scherrer equation.

3.3.7 Electron spin resonance (ESR)

The surface Ti^{3+} on TiO_2 surface were measured by electron spin resonance spectroscopy (ESR) which conducted at power 1mW and amplitude 2.5x100 without illumination using a JEOL, JES-RE2X. it was performed to monitor the surface Ti^{3+} on the surface of the TiO_2

3.4 Catalyst activity on CO oxidation reaction

The CO oxidation was performed in a 5 mm i.d. quartz tubular fixed bed microreactor. The reactant and product were analyzed on-line with a Shimadzu GC-8ATP gas chromatograph equipped with a thermal conductivity detector (TCD) and a Porapak Q column with He carrier gas. The experimental operating conditions are given in appendix C. A flow diagram of catalytic CO oxidation reactor system is show in **Figure 3.1**. The reactant feed contained 1% CO and 2% O_2 by volume with He balanced was through the catalyst bed at total gas flow rate of 50 cm^3 min^{-1}. Inlet gas composition was controlled by mass flow meter. The procedures of the catalytic testing as show below.

3.4.1 Approximately 50 mg of metal catalyst was loaded onto the tubular reactor and the catalyst bed was held by quartz wool.

3.4.2 The tube was placed inside a temperature controlled oven.

3.4.3 A thermocouple was inserted into the tube with one end touching the catalyst zone in order to measure the bed temperature.

3.4.4 Before CO oxidation reaction, the catalyst was first reduced in-situ at 500°C for 1h in Hydrogen flow rate 50 cm^3/min then heat up to 510°C in Helium flow and cool down to room temperature.

3.4.5 The reactant gas was switched to reactor. The temperature of oven was heated from room temperature to desired temperature with heat rate 2 °C/min.

3.4.6 The composition of reactant and product were analyzed by Shimadzu GC-8ATP gas chromatograph.

Catalytic activity was evaluated in term of the light-off temperature, defined as the temperature at 50% conversion was obtained. The calculation of CO conversion was based on CO consumption, determined by using the following equation (3.1).

$$\%CO\ Conversion = \frac{(CO_{in} - CO_{out})}{CO_{in}} \times 100 \qquad (3.1)$$

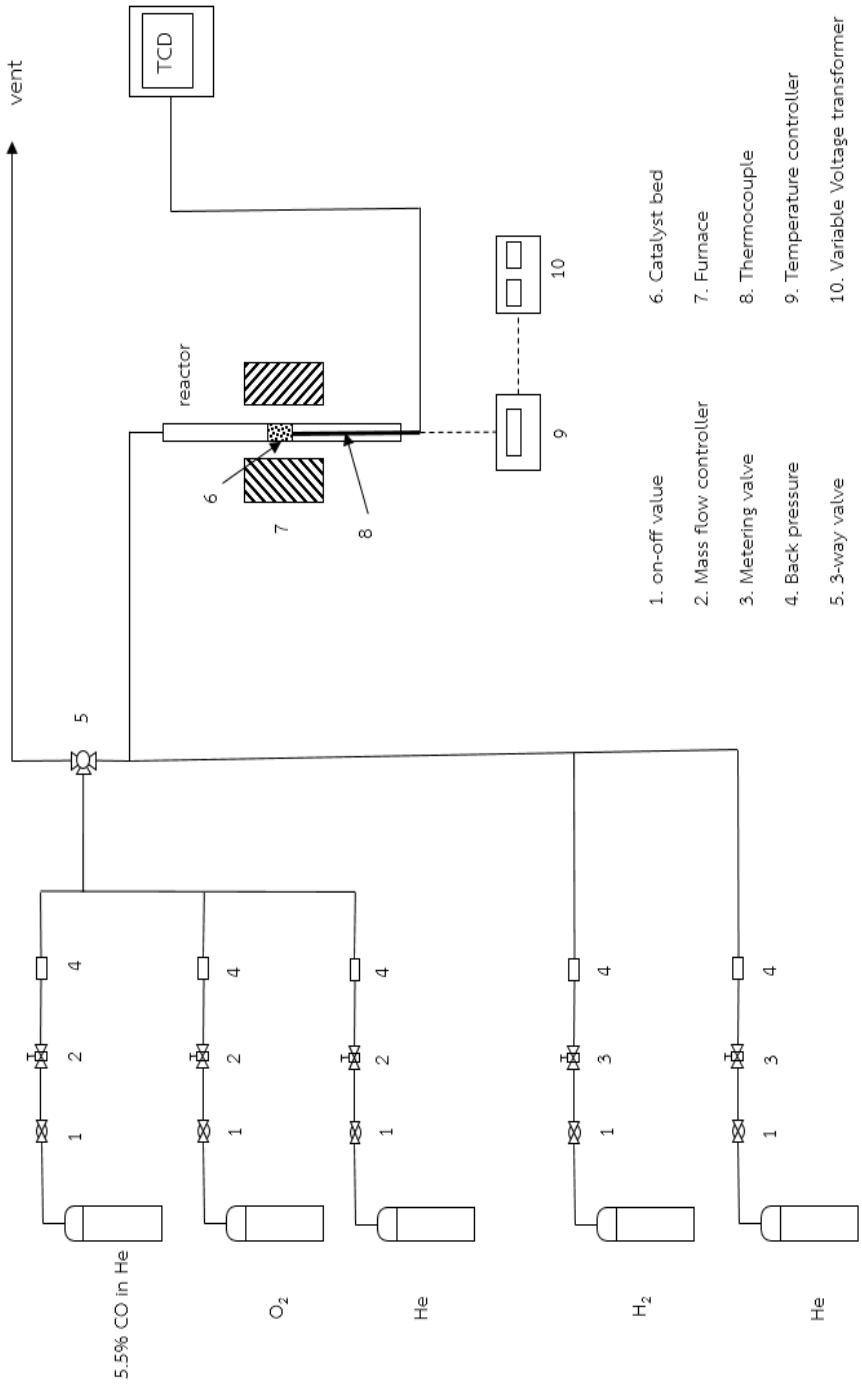

Figure 3.1 Flow diagram of the system for testing catalytic activity

CHAPTER IV
RESULTS AND DISCUSSION

The results and discussion in this chapter consist of two parts, including the effect of yttria (Y/Ti malar ratio 0.001, 0.005, 0.01, 0.05, 0.1) modified TiO_2 on Pt dispersion and CO oxidation activity of Pt/TiO_2 and the second part, the effect of other transition metals (Zr, Nb, La) modified TiO_2. The catalyst characteristics were investigated by N_2-physisorption, XRD, H_2 temperature program, XPS, ESR, TEM and Pt dispersion which was estimated by CO pulse chemisorption technique. The catalytic properties of Pt catalysts supported on transition metals modified TiO_2 supports were investigated in CO oxidation reaction.

4.1 The effect of yttria (Y/Ti malar ratio 0.001, 0.005, 0.01, 0.05, 0.1) modified TiO_2 on Pt active sites and CO oxidation activity of Pt/TiO_2

The Pt catalyst on yttria modified TiO_2 with various molar ratios of Y/Ti in the range of 0.001-0.1 were prepared by successive impregnation method and denoted as $Pt/0.001Y\text{-}TiO_2$, $Pt/0.005Y\text{-}TiO_2$, $Pt/0.01Y\text{-}TiO_2$, $Pt/0.05Y\text{-}TiO_2$, and $Pt/0.1Y\text{-}TiO_2$.

4.1.1 Effect of different dopant ratios on the properties of $Pt/Y\text{-}TiO_2$

4.1.1.1 N_2 physisorption

The BET surface area, pore volume, average pore size diameter and N_2 adsorption-desorption isotherm of $Pt/Y\text{-}TiO_2$ catalyst by low temperature nitrogen technique are shown in **Table 4.1**. It is evident that BET surface area, pore volume, and average pore diameter were slightly decreased with increasing Y/Ti ratios. This can be due to the fact that doped yttria cover surface and pore of the TiO_2. **Figure 4.1** shows the N_2 adsorption-desorption isotherms of Pt/TiO_2 and $Pt/Y\text{-}TiO_2$ as a type IV isotherm with a hysteresis loop. There catalysts were mesoporous materials with pore diameter in the range of 2 to 50 nm [69].

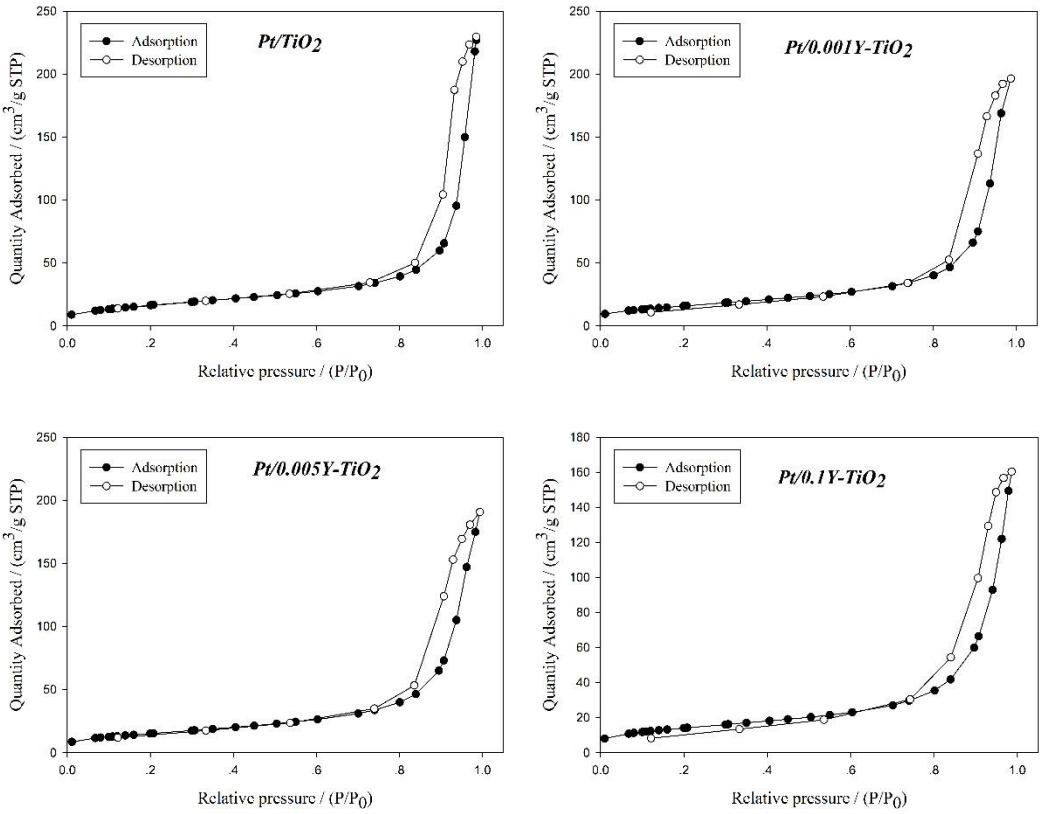

Figure 4.1 N_2 adsorption-desorption isotherm of Pt/TiO_2 and $Pt/Y\text{-}TiO_2$

Table 4.1 Physical properties of Pt/TiO_2 and $Pt/Y\text{-}TiO_2$

Catalysts	BET surface Area (m^2/g)	Pore Volume[a] (cm^3/g)	Average Pore size[a] (nm)
Pt/TiO_2	61	0.35	20
$Pt/0.001Y\text{-}TiO_2$	55	0.30	17
$Pt/0.005Y\text{-}TiO_2$	56	0.30	17
$Pt/0.1Y\text{-}TiO_2$	51	0.25	17

[a] calculated by BJH method (desorption branch)

4.1.1.2 X-ray Diffaction (XRD)

The structural phase of TiO_2 and yttria modified TiO_2 supported Pt catalysts were charcterization by X-ray diffraction technuque using using Cu K_α irradiation at

range between 20° and 80° with a step of 0.05° s^{-1}. Broadening and position of the diggraction peaks were used to estimate crystallite diameter.

The X-ray diffraction patterns are shown in **Figure 4.2**, all the sample exhibited similar peaks, showing only anatase and rutile TiO_2. The peaks position at 2θ degrees 25.3, 38, 48.1, 55 and 62.5° can be attributed to the diffraction planes of anatase TiO_2 and the peaks at 2θ degrees 27.5, 36, 54 and 69° can be attributed to diffraction planes of rutile phase of TiO_2 [70]. The characteristic peaks corresponding to yttrium oxide phases were not detected due probably to well distribution of the yttrium oxide which could not be detected by XRD. Platinum species were also not detected due to their well dispersed and the very low amount present. The intensity decreasing of crystallinity of TiO_2 were observed when the amount of yttria was increased which suggested that Y had interacted with TiO_2 and covered the surface of TiO_2 [71]. The low intensitiy and broad peak in Pt/0.005Y-TiO_2, Pt/0.05Y-TiO_2 and Pt/0.1Y-TiO_2 prossibly suggest that amorphous or larger atom of yttria on TiO_2 surface might acted as an X-ray scatterer which led to lower intensity and position peak of anantase (1 0 1) shift from 2θ = 25.32° to lower degree [72]. The crystallite size of TiO_2 by Scherrer's equation and the ratio phase of anatase to rutile are shown in **Table 4.2**. However, Scherrer equation assume that the lattice defects (inhomogeneous strain and crystal lattice imperfections) of the paritcle are negligible which value error from theory. Especially, in range 0.05-0.1 Y/Ti ratios.

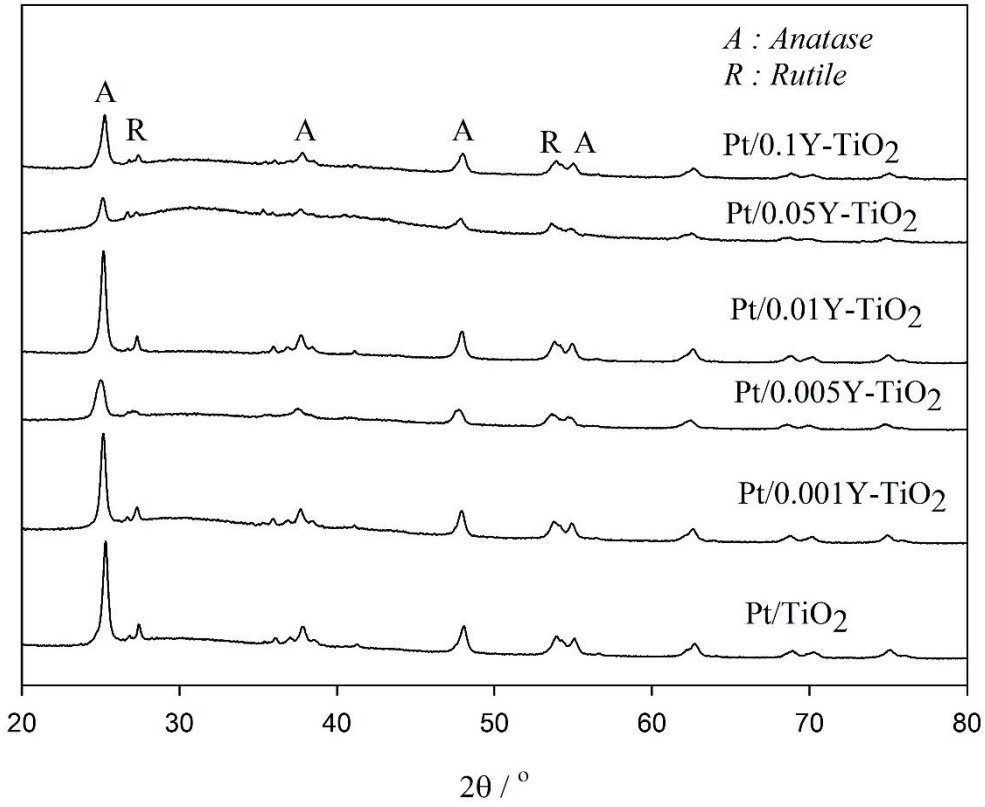

Figure 4.2 XRD patterns of Pt/TiO_2 and $Pt/Y\text{-}TiO_2$

Table 4.2 XRD analysis results of yttria modified TiO_2 supported Pt catalysts

Catalyst	Crystallite size of anatase TiO_2* (nm)	Ratio phase anatase to rutile
Pt/TiO_2	26	3.68
$Pt/0.001Y\text{-}TiO_2$	26	3.60
$Pt/0.005Y\text{-}TiO_2$	13	3.07
$Pt/0.01Y\text{-}TiO_2$	18	4.62
$Pt/0.05Y\text{-}TiO_2$	23	3.65
	$Pt/0.1Y\text{-}TiO_2$	3.42

* The crystallite size of TiO_2 based on the Scherrer equation

4.1.1.3 CO chemisorption

The active sites of platinum catalysts were measured by CO-pulse chemisorption technique based on an assuption that one carbon monoxide adsorbs on one plantinum site by one molecule CO

The 0.001-0.05 Y/Ti mole ratio of Y-modified TiO_2 supported Pt catalysts showed higher amount of Pt active sites than the unmodifiend TiO_2 supported (Figure 4.3.). The highest Pt active sites was obtained at Y/Ti = 0.001 and declined as the Y/Ti ratio was further increased. The excess yttria probably cover Pt or Pt low distibutes over yttria led to lower active sites (Y/Ti = 0.1). Excess dopant might encumber on surface and led to lower active sites.

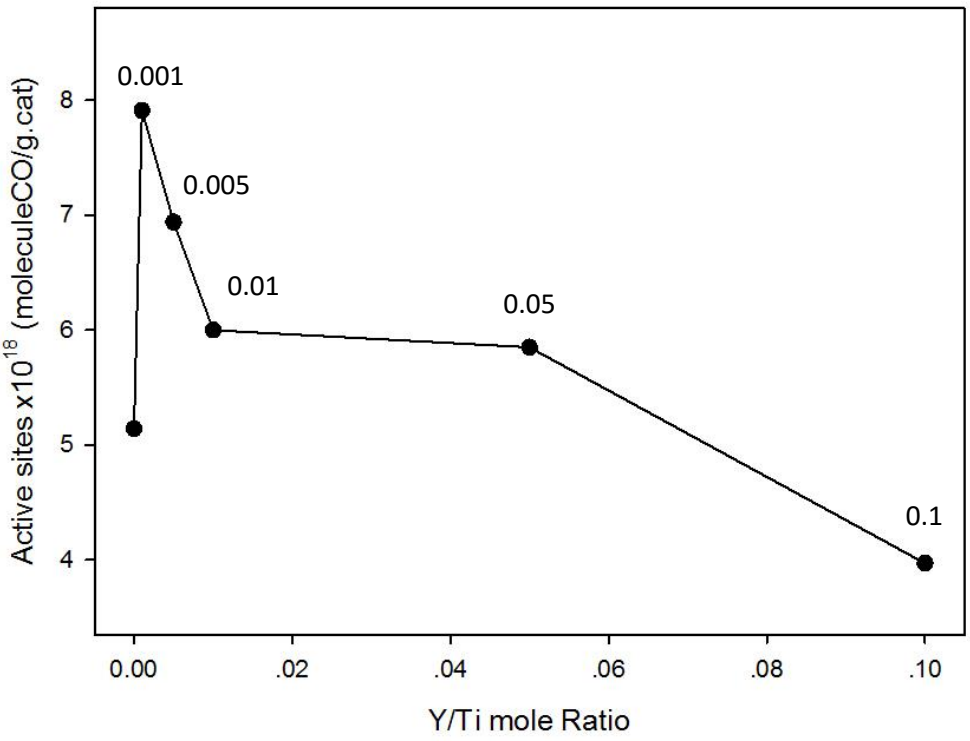

Figure 4.3 Effect of Y/Ti ratio on Pt active sites of the Pt/Y-TiO2 catalyst

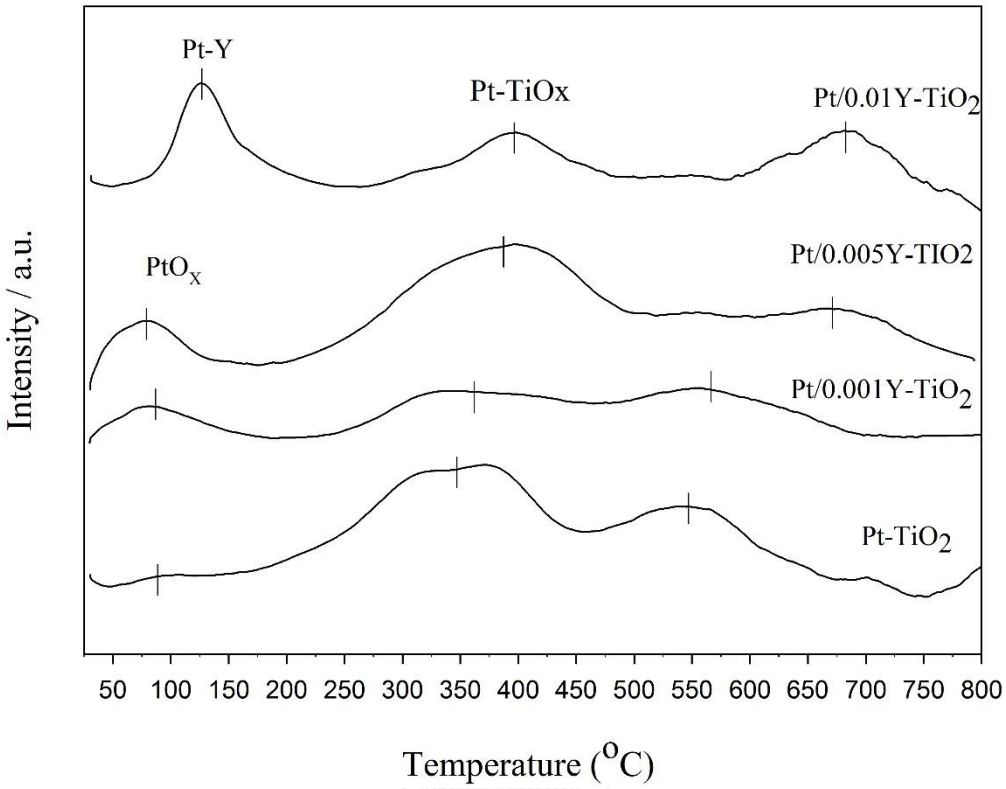

Figure 4.4 H_2-TPR of Pt/Y-TiO_2 Catalysts

4.1.1.4 H_2 temperature program reduction

The reduction behaviors of the Pt/Y-modified TiO_2 were investigated by H_2-TPR and the results are shown in **Figure 4.4**. The catalysts exhibited three reduction peaks at approximately 100, 300-500, >500°C. The peak at 100°C could be assigned to the reduction of Pt oxide particles [5, 73]. The reduction of PtO_x in Pt-TiO_2 showed low intensity due to partial reduction of oxides support and noble metals supported on TiO_2 were known to exhibit strong metal-support-interaction (SMSI) [74]. The addition of second metals could significantly increase the Pt reducibility and have an impact on the reduction temperature of Pt [74, 75] or interacted with Pt species. The second peak at 300-500°C were attributed to the reduction of the surface or surface particles by hydrogen spillover effect [5, 73] or the reduction of Pt species interacting with the

TiO_2 support [76]. The third appeared over 500°C was assigned to reduction of bulk TiO_2 [77].

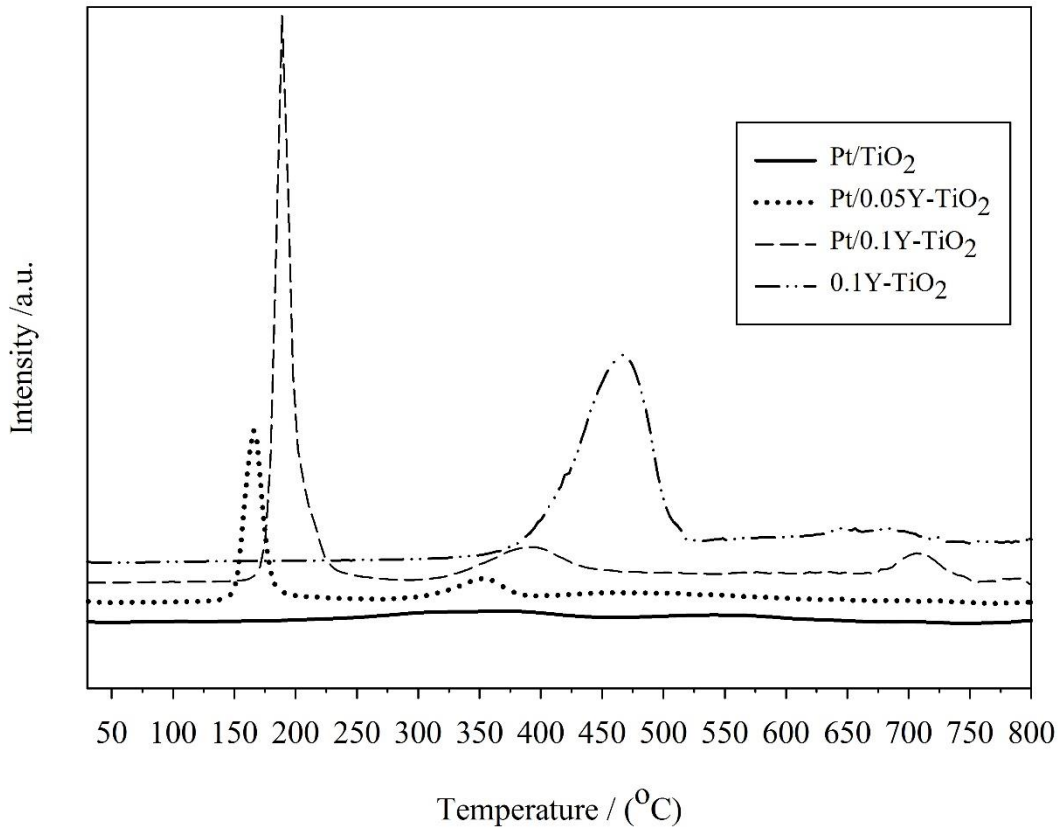

Figure 4.5 H_2-TPR of Y-TiO_2 support and Pt/Y-TiO_2 Catalysts with high Y/Ti ratios

It is known that yttrium is a non-reducible or less reducible support [78]. From **Figure 4.5**, it can be observed the peak of 0.1Y-TiO_2 at 475°C which is the reduction of yttria interact with titania support. Yttrium modified titania support Pt/0.05Y-TiO_2 and Pt/0.1Y-TiO_2 showed the reduction peak of yttria approximately at 500°C which may possibly be attributable to the reduction temperature of transition metals which was shifted to lower temperature when doped with noble metals [74, 79] as compared to the Y-TiO_2 support. The intensive peak approximately at 200°C may be attributed to yttria interacted with Pt and this peak shifted to lower reduction temperature. The

PtO_x reduction in Pt/0.1Y-TiO_2 was not observed because of very low intensity of Pt compared with the reduction peak of yttria.

4.1.1.5 X-ray photoelectron spectroscopy (XPS)

The electronic states and surface compositions of Y-modified TiO_2 supported Pt catalysts were investigated by X-ray photoeletron spectroscopy (XPS). The binding energy spectra of Ti 2p, Y 3d and Pt 4f were used to evaluate the effect of dopant on TiO_2 support and platinum, to understand the characteritics of plantinum, oxygen, titania and yttria species on the catalyst surface.

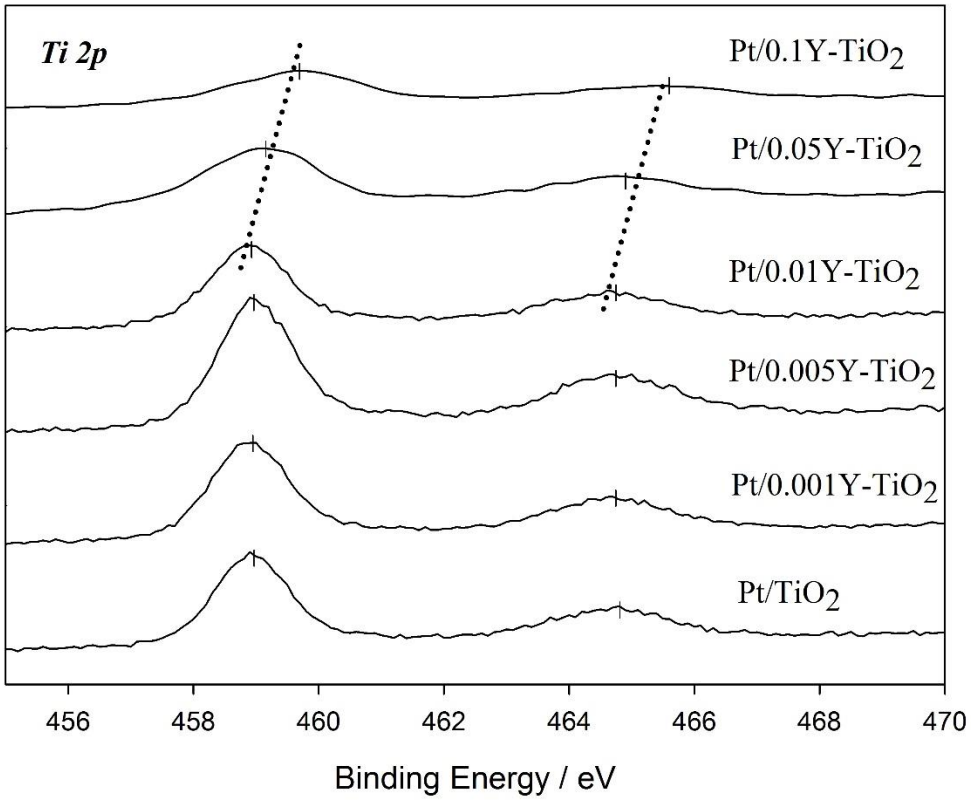

Figure 4.6 XPS spectra of Ti 2p for Pt/TiO_2 and Pt/Y-TiO_2

Figure 4.6 showed binding energy approximately at 458.9 ev and 464.7 eV, which were assigned to $2p_{3/2}$ and $2p_{1/2}$ states of Ti^{4+} in TiO_2 [80]. The Ti^{3+} was not

clearly detected at 457.5 and 463.2 eV [81] due to low amount of Ti^{3+}. The binding energy shifted to higher values when Y/Ti ratios increased from 0.01 to 0.1 which may be ascribed to the yttria-titania interaction as also confirmed by the H_2 TPR results. The weak intensity may be due to yttria cover TiO_2 support. The peaks at 457.5 and 463.2 eV were appeared in Pt/0.05Y-TiO_2, which indicated that yttria addition increased Ti^{3+} in TiO_2 as shown in **Figure 4.7.**

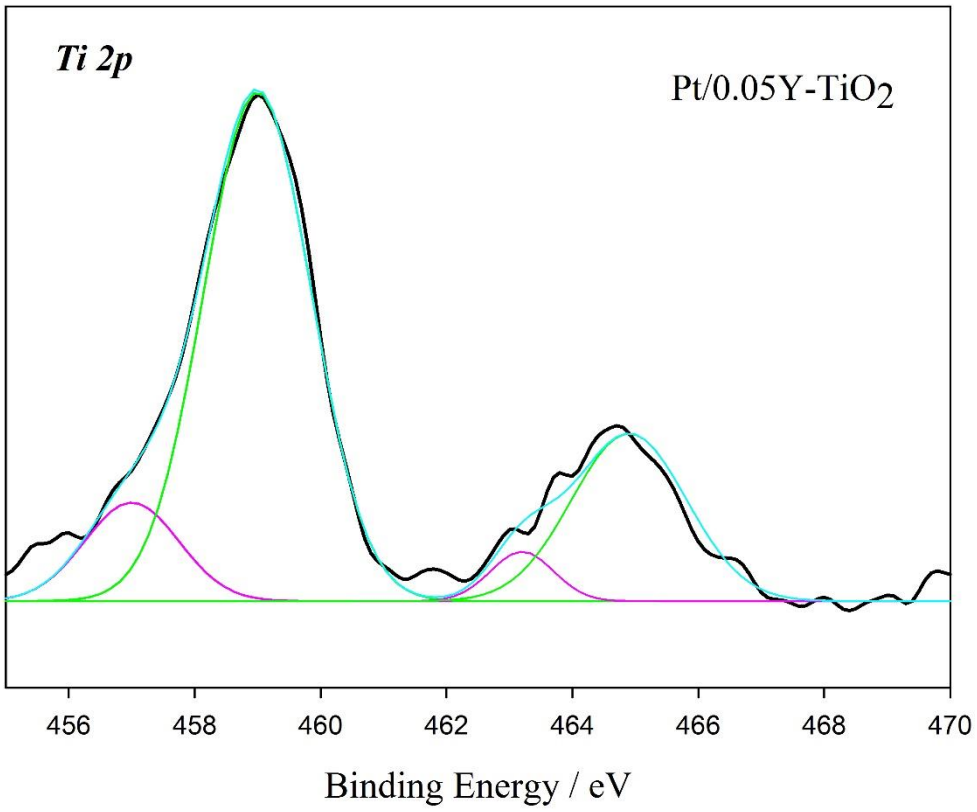

Figure 4.7 XPS spectra of Ti 2p for Pt/0.05Y-TiO_2

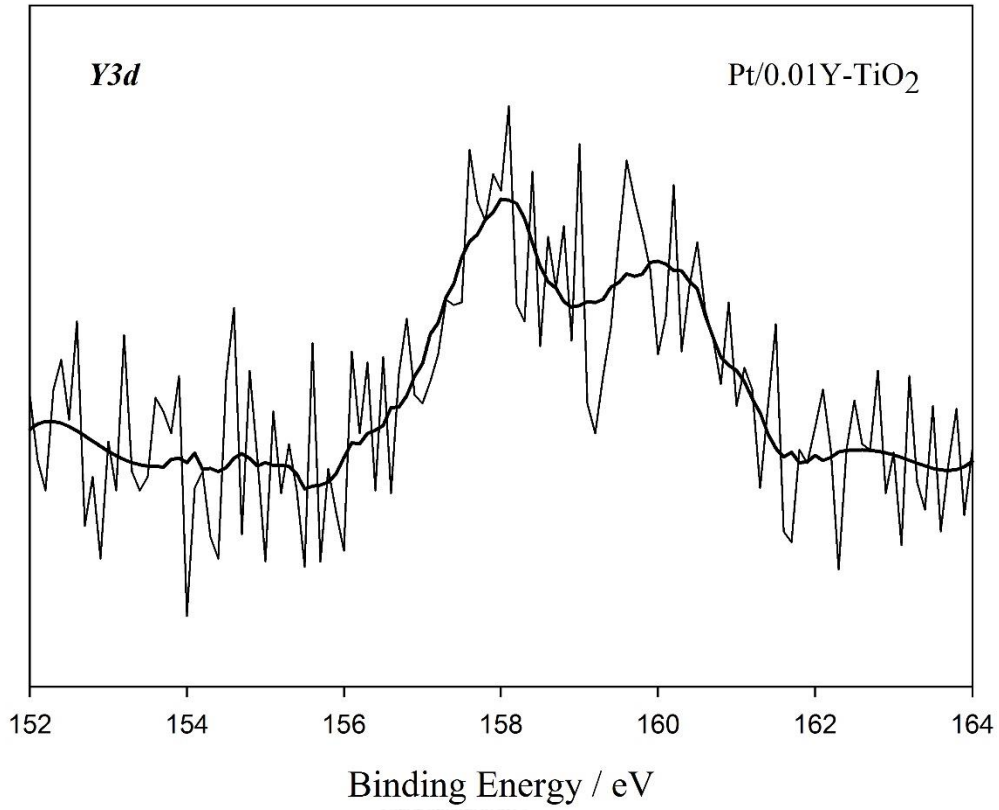

Figure 4.8 XPS spectra of Y3d for Pt/0.01-TiO_2

The Y 3d peaks of Pt/0.001 Y-TiO_2 were found at binding energies 158 eV and 160.0 eV as shown in **Figure 4.8,** which were higher than those of Y_2O_3 support materials (3d5/2: 156.8 eV, 3d3/2: 158.7 eV) [20]. It was reported that Y 3d peaks at 157.9 eV and 160 eV are Y^{3+} $3d_{5/2}$ and Y^{3+} $3d_{3/2}$, respectively which could be attributed to Y^{3+} substitute into Ti^{4+} in TiO_2 lattice [82, 83]. However, it is unconvincing in this case because the catalyst were prepared by impregnation method and the ionic radius of Y^{3+} (90pm) is larger than Ti^{4+}, which is only 68pm [84]. Thus, it is hard for Y^{3+} to substitute in Ti^{3+} lattice. The shift of binding energy was conjectured that yttria species may exhibit strong interactions with titania and cause electron binding energy deviation [20].

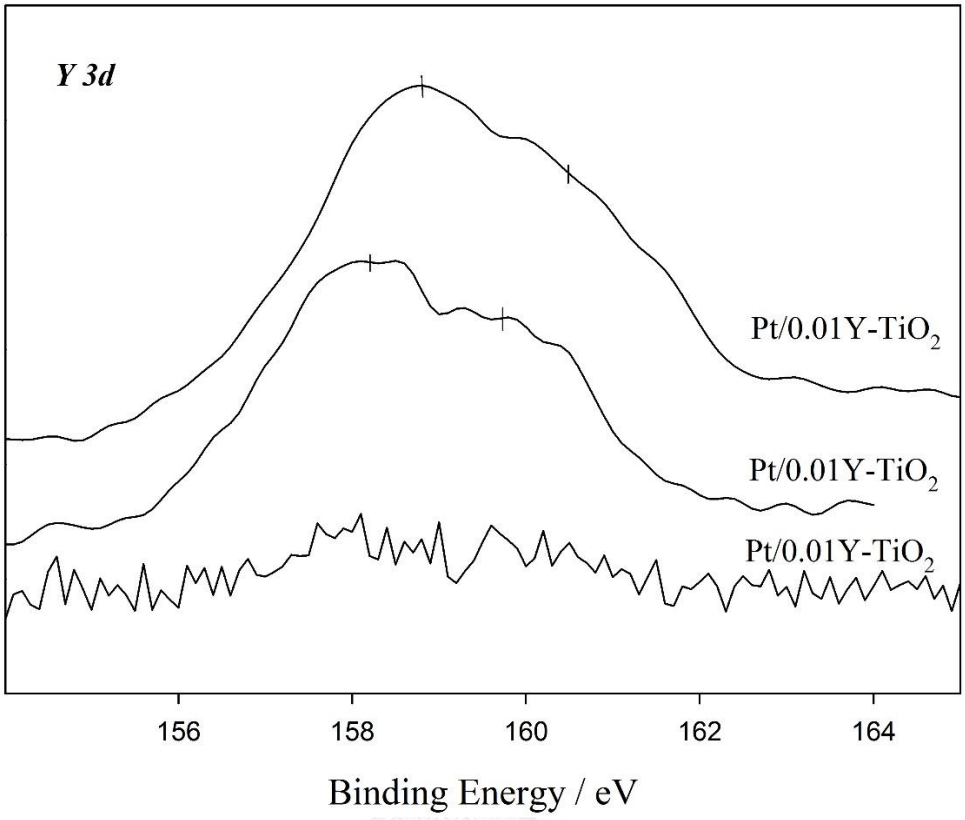

Figure 4.9 XPS spectra of Y 3d for Pt/Y-TiO_2 with 0.01-0.1 Y/Ti mole ratios

As shown in **Figure 4.9**, the Y 3d binding energy increased with increasing Y/Ti ratio from 0.01 to 0.1 because of the yttia-titania interaction or yttria-platinum interaction corresponding to the reduction behaviors.

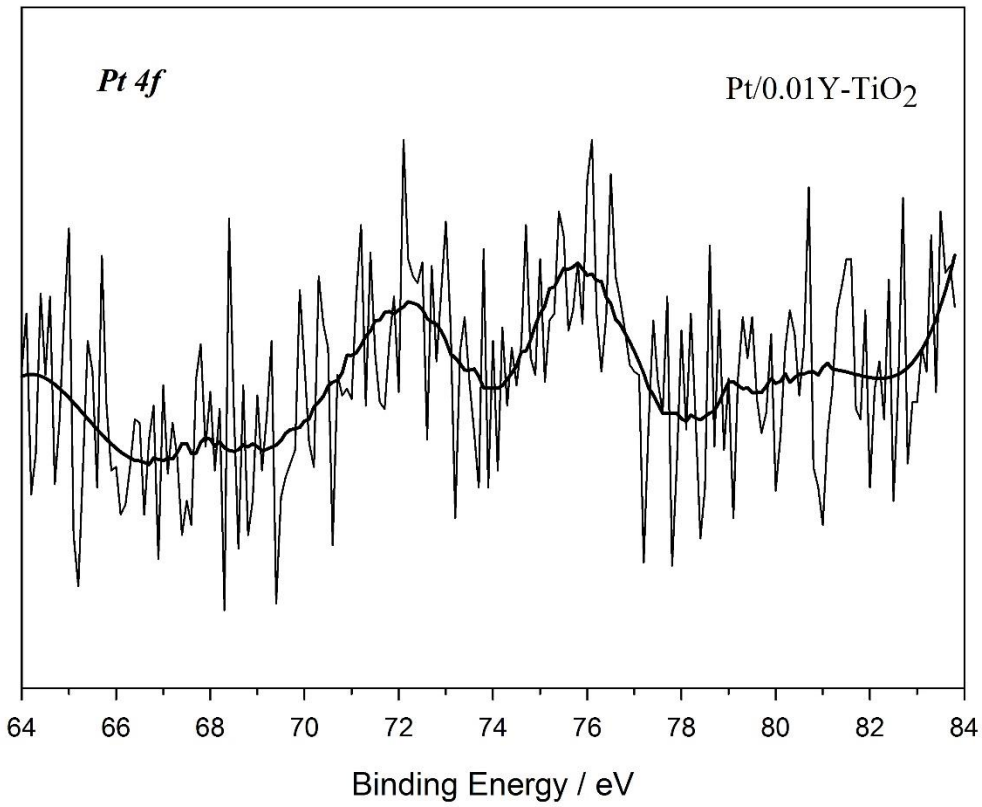

Figure 4.10 XPS spectra of Pt4f for Pt/0.01-TiO_2

The spectra of Pt 4f are shown as two peaks at around 72.5 and 75.8 eV in **Figure 4.10**, which can be assigned to PtO [20]. It was found that addition of yttria led to easier observation of PtO_x in the Pt/TiO_2, It is suggested that the yttria doping increased Pt dispersion or encouraged platinum to be in PtO_x after calcination. The XPS was consistent with the corresponding H_2 TPR results.

4.1.1.6 Electron spin resonance (ESR)

ESR signals of trapped electrons and holes on TiO_2 and Y-TiO_2 at 130K are shown in **Figure 4.11**. the sharp signals at g = 1.975 was assigned to lattice electron trapping site (Ti^{3+}) in Degussa P25 due to rutile phase and signal at g = 1.990 was

assigned to lattice electron trapping site in anatase phase [85, 86]. It was reported that Ti^{3+} signal of anatase phase in Degussa P25 clearly appear under UV illumination condition [85, 86]. Yttria doped TiO_2 exhibited increasing of Ti^{3+} in TiO_2 as also confirmed by Ti 2p spectra of Pt/0.05Y-TiO_2, shown in **Figure 4.7**. The highest signals were observed for the 0.001Y-TiO_2 and decreased when increase Y/Ti ratio. The ESR results showed a similar trend as CO chemisorption results in **Figure 4.3**. It is suggested that Ti^{3+} defect was related to metal dispersion.

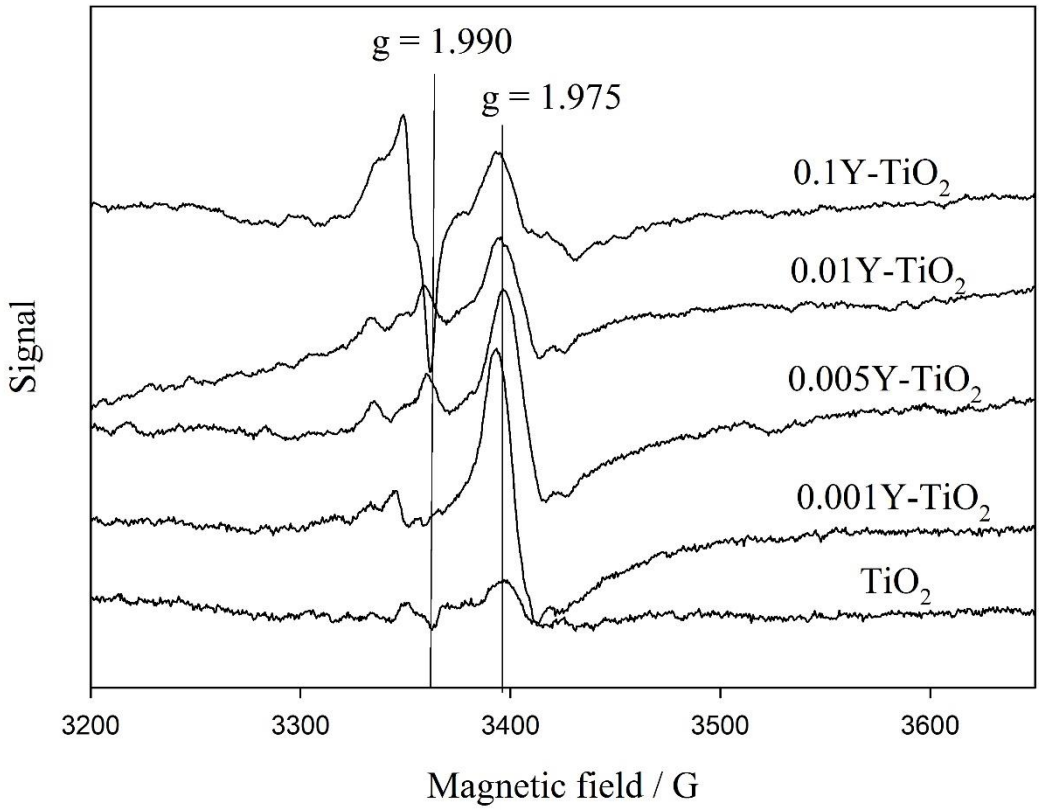

Figure 4.11 ESR spectra of Pt/Y-TiO_2 at 130K

4.1.1.7 Transmission electron microscope (TEM)

The TEM images and size distribution of Pt/TiO_2, 0.001Y-TiO_2 and 0.1Y-TiO_2 are shown in **Figure 4.12-4.17**. The Pt particles were not clearly detected in all sample due to low amount of Pt loading and highly distribution. The size average of TiO_2,

0.001Y-TiO_2 and 0.1Y-TiO_2 support from 100 particle samples were 24, 23, and 24 nm, respectively. The particle size on Pt/0.1Y-TiO_2 calculated by Scherrer equation (21 nm) was larger than average particle size by TEM image due to scattering effect. It is conjecture that loading Pt and Y had no effect on the TiO_2 crystallite size.

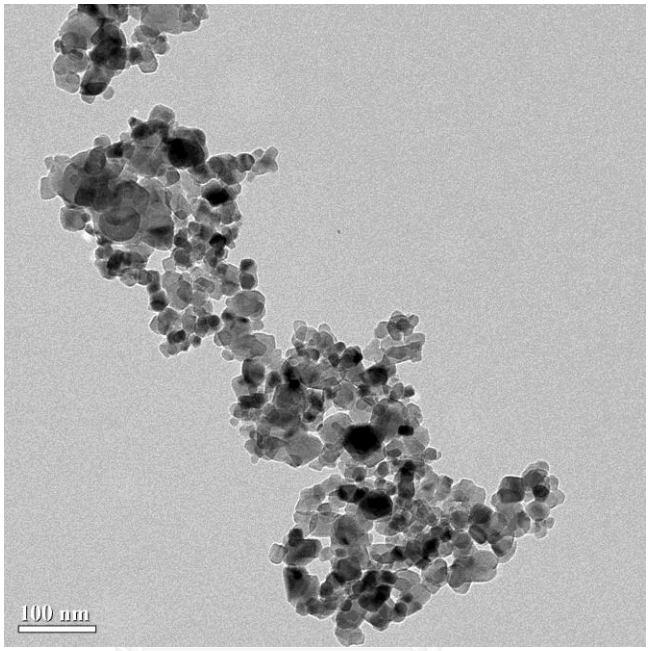

Figure 4.12 TEM image of Pt/TiO_2

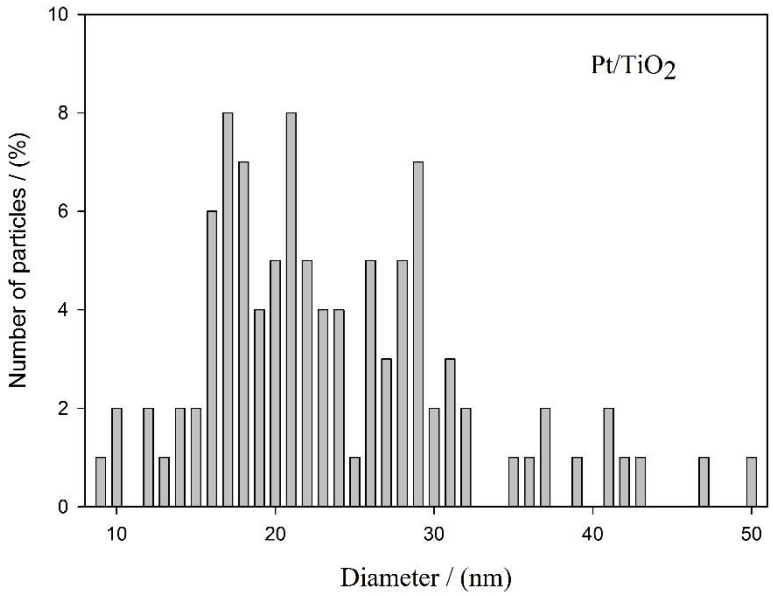

Figure 4.13 size distribution of Pt/TiO_2

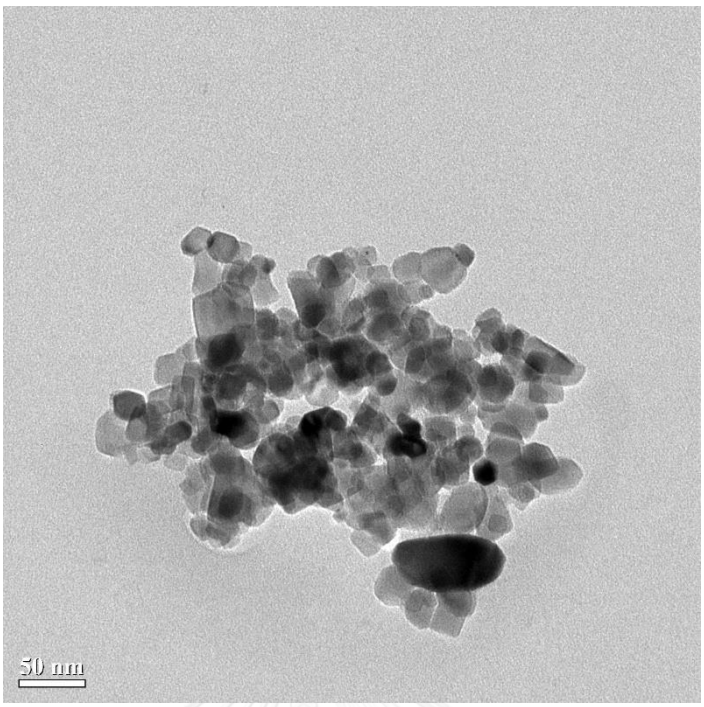

Figure 4.14 TEM image of Pt/0.001Y-TiO_2

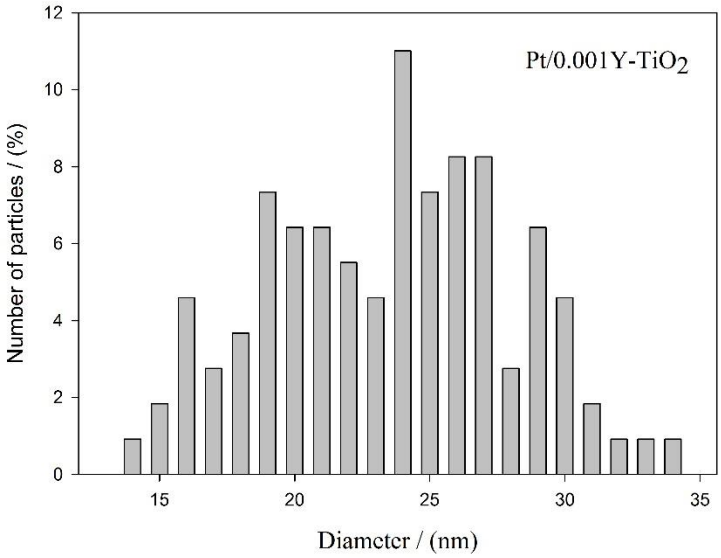

Figure 4.15 size distribution of Pt/0.001Y-TiO_2

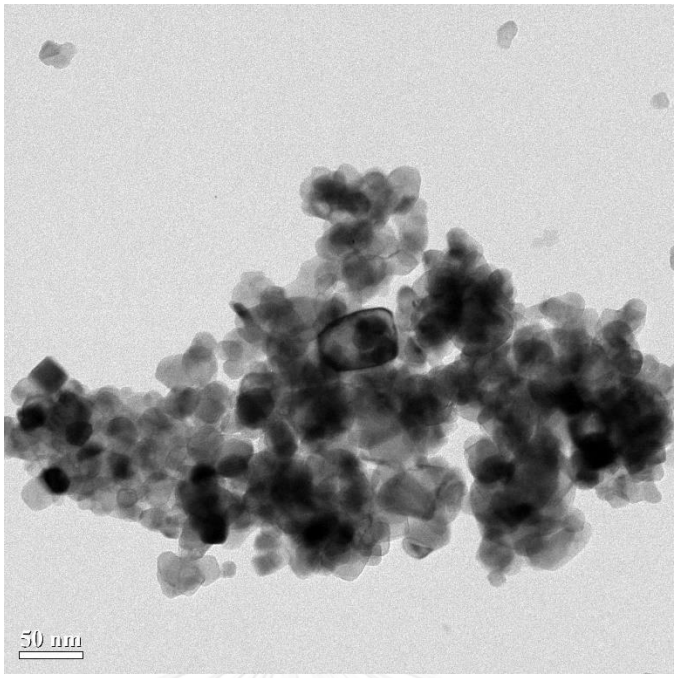

Figure 4.16 TEM image of Pt/0.1Y-TiO_2

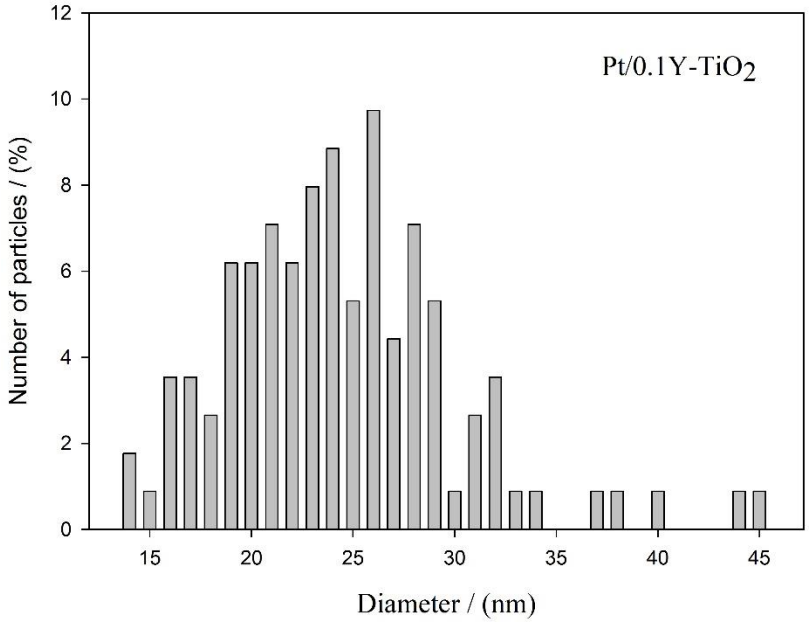

Figure 4.17 size distribution of Pt/0.1Y-TiO_2

The TEM images of Pt/0.001Y-TiO_2 and Pt/0.1Y-TiO_2 are shown in **Figure 4.14, 4.16**. In the both images, yttria particle were not found. However, For the Pt/0.1Y-TiO_2, the presence of yttria species was confirmed by EDX analysis, as shown in **Figure 4.18**.

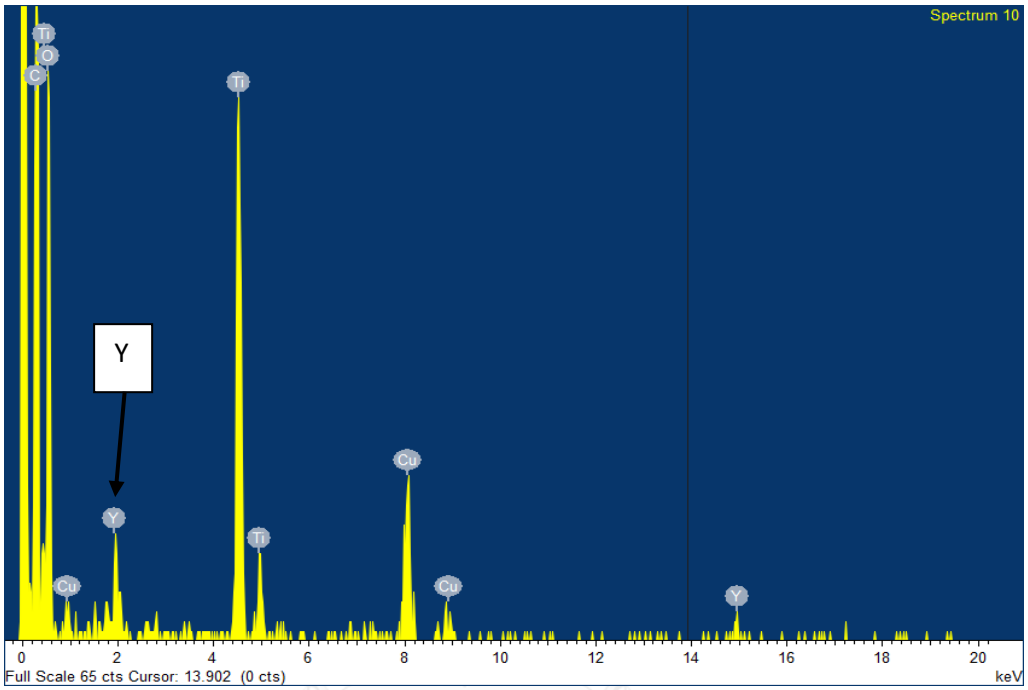

Figure 4.18 TEM-EDX analysis of Pt/0.1Y-TiO_2

4.1.2 Effect of different dopants on the activity of CO oxidation

The catalytic performances of yttria modified TiO_2 supported Pt in CO oxidation are shown in **Figure 4.19**. It is revealed that CO conversion was improved by modifying the TiO_2 supports with Y dopants at Y/Ti ratios in the range of 0.001-0.005 due to increasing of metal active sites. The Pt/0.001Y-TiO_2 catalyst exhibited the lowest light-off temperature at 85.8°C at 50% CO conversion and the Pt/0.005Y-TiO_2 showed the light-off temperature of 103.2°C. Both values were lower than that of the unmodified Pt/TiO_2 (light-off temperature 107.8°C). However, further increase Y/Ti ratio to 0.01 resulted in lower catalytic activity of the Pt/0.01Y-TiO_2 and Pt/0.05Y-TiO_2 despite its higher Pt active sites compared to the unmodified Pt-TiO_2. The light-off temperatures were at 112.2°C and 162.6°C, respectively.

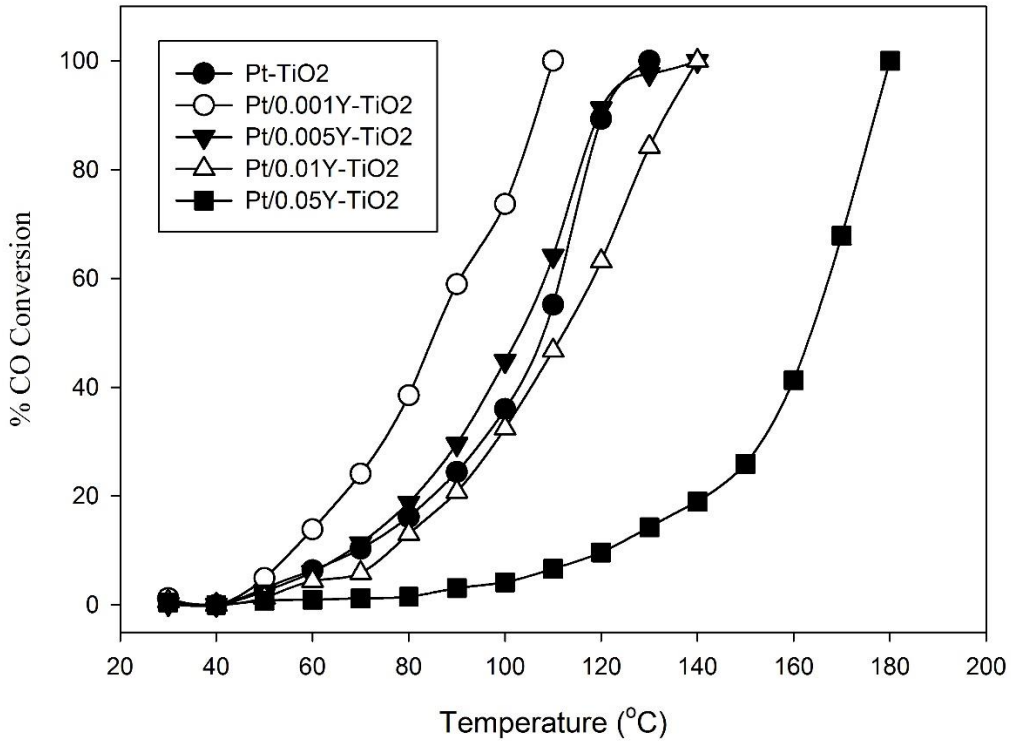

Figure 4.19 CO conversion over Pt/Y-TiO_2 and unmodified Pt/TiO_2

CO oxidation on supported metal catalysts was widely accepted to occur via the following Langmuir-Hinshelwood mechanism which both carbon monoxide and oxygen competitive adsorbed on same adsorption sites. X. Ouyang and S. Scott [60] reported that CO oxidation on Pd-substituted $BaCeO_3$ in excess oxygen condition, the kinetic show CO inhibition. However, the noble metals supported on reducible oxides like CeO_2, TiO_2, Fe_2O_3 and Co_3O_4 exhibit high reactivity for CO oxidation. It is suggested that Mar-Van Krevelen mechanism is expected to take place together with the Langmuir-Hinshelwood mechanism [87, 88]. Thus, the catalytic results can be explained by Mars-Van Krevelen mechanism. The CO molecule is adsorbed on metal active sites to form intermediate complex and then reacted with surface lattice oxygen atoms perimeter of the Pt-TiO_2 interface to generate CO_2. The oxygen lattice was refilled by external oxygen, oxygen in gas phase dissociates into atomic oxygen and adsorbed on the oxygen vacancies sites of TiO_2 support. Following Eq. (1.1-1.4) [88],

doping Y could create defect sites on TiO_2 which improved TiO_2 support to activate O_2 and reacted with the nearly CO activated on Pt particles. However, the lower activity on increasing yttria dopant could be due to the ratio of presence of yttria cover TiO_2 surface corresponding to decreasing of oxygen surface. The $O_{surface}/O_{lattice}$ show in **Table 4.3**. Pt probably deposited on yttria surface. Thus, the CO adsorbed on Pt could not react with the nearly oxygen in TiO_2 lattice.

Table 4.3 surface oxygen to lattice oxygen ratio by O 1s spectra

sample	$O_{lattice}$	$O_{surface}$	$O_{surface}/O_{lattice}$
Pt/TiO_2	530.1	531.9	0.2374
Pt/0.001Y-TiO_2	530.1	531.8	0.2352
Pt/0.005Y-TiO_2	530.2	532.2	0.2092
Pt/0.01Y-TiO_2	530.1	532.1	0.1690

The turnover frequency (TOF) of Pt/Y-TiO_2 with different doping ratios are shown in **Figure 4.20**. Only the TOF of Pt/0.001Y-TiO_2 was found to be higher than that of the unmodified Pt/TiO_2. This suggests that yttria doped TiO_2 increased metal active sites, which was conjectured particle size decreasing, but decreased activated oxygen on catalyst surface which lead to lower TOF when increasing yttria dopant.

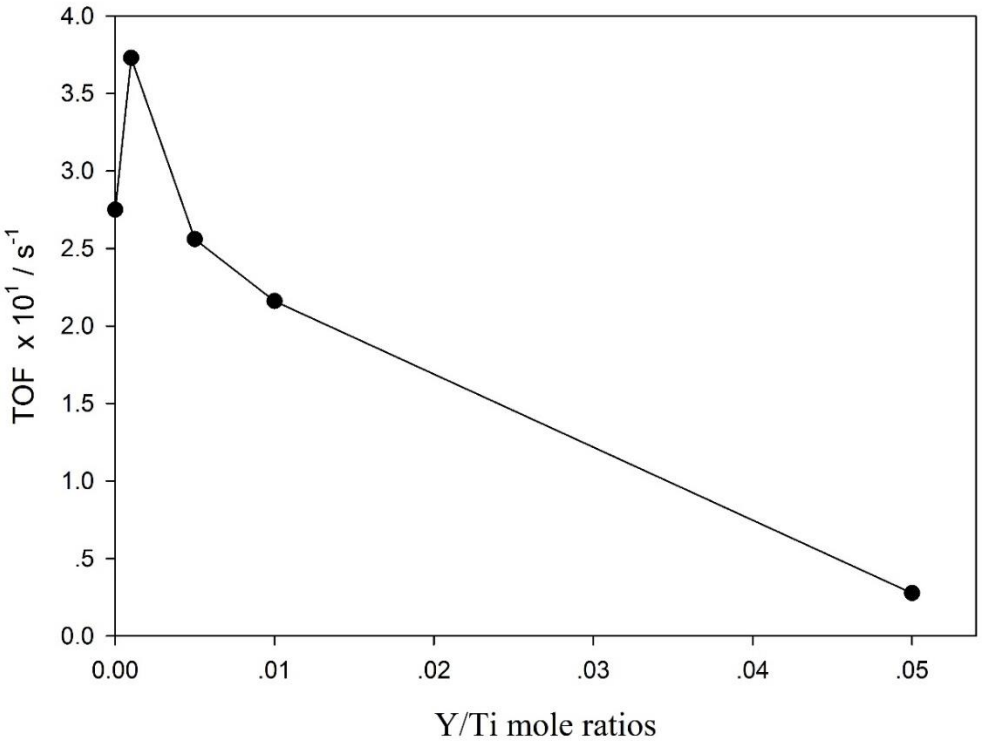

Figure 4.20 Turnover frequency (TOF) of Pt/Y-TiO_2 with different doped ratios at 100 ℃

N. Li [5] investigated the effect of Pt particle sizes (Pt/TiO_2) on the CO oxidation. They reported that turnover frequencies based on Pt dispersion varied as declined with increasing Pt particle size. However, turnover frequency based on Pt atoms located on the periphery of Pt–TiO_2 interface remained constant at 40°C, implying that these periphery Pt atoms were the active sites. Thus, we conjectured that the increasing of active sites on yttria doped TiO_2 supported Pt due to decreasing of Pt particle size, which led to higher TOF. The lower TOF because periphery Pt atoms located on yttria which could not react with the nearly oxygen lattice on TiO_2.

4.2 The effect of different transition metal Y, La, Nb and Zr (M/Ti malar ratio 0.001, 0.005, 0.01, 0.05, 0.1) modified TiO_2 on Pt dispersion and CO oxidation activity of Pt/TiO_2

4.2.1 Effect of different dopant ratios on the properties of $Pt/M\text{-}TiO_2$

4.2.1.1 CO chemisorption

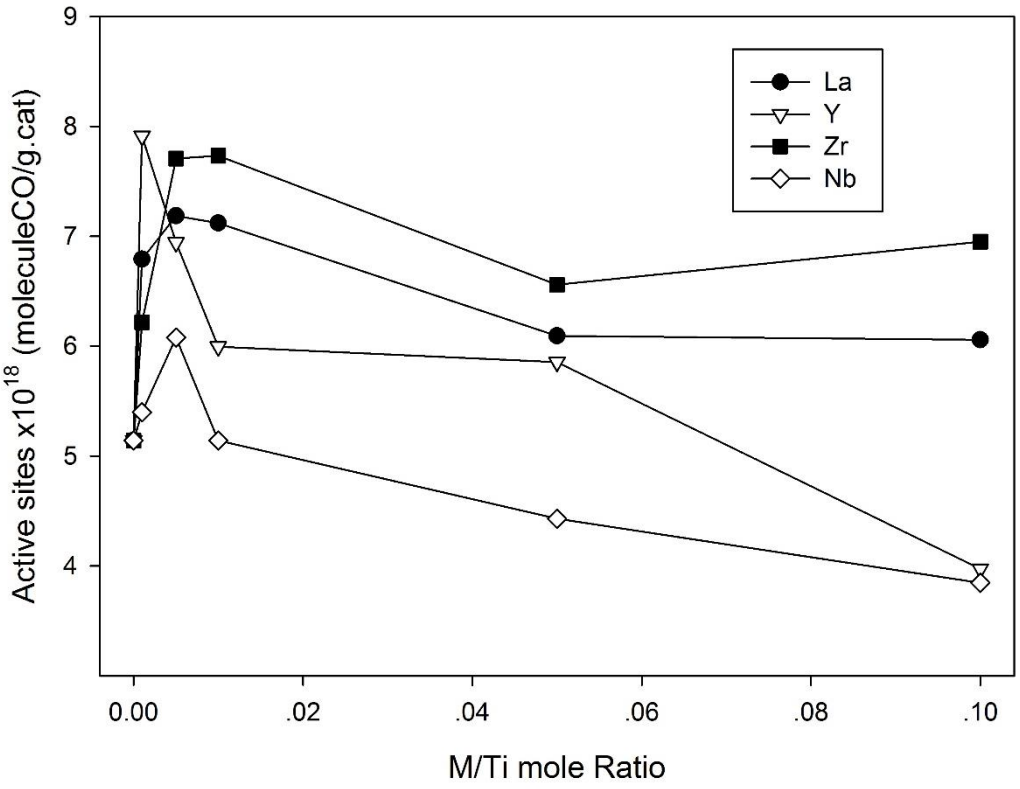

Figure 4.21 Effect of varies ratio of transition metals on Pt active sites

The effect of transition modified TiO_2 supported Pt on active sites with M/Ti ratios 0.001-0.1 is shown in **Figure 4.21**. It was observed that 0.005 ratios of La, Zr and Nb showed the highest Pt active sites. Nevertheless, Pt active sites on 0.1 ratio of Zr and La was not decreased. It is suggested that Pt can be better dispersed on Zr and La surface than TiO_2 and Y and Nb modified TiO_2.

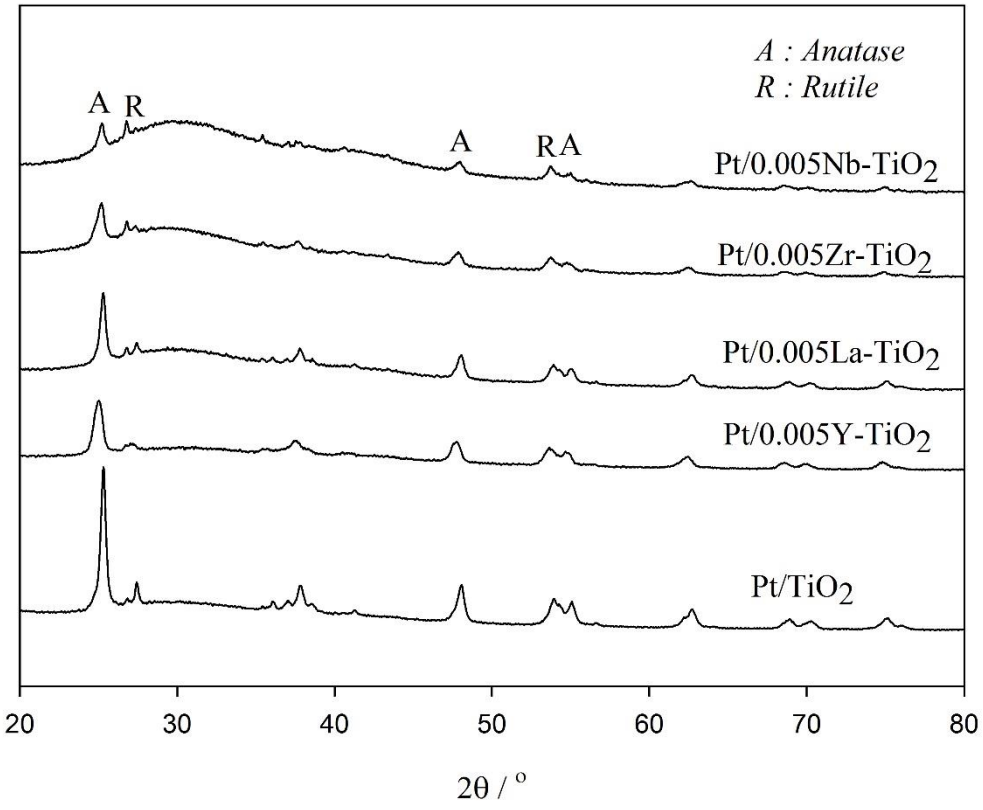

Figure 4.22 XRD pattern of Pt/0.005M-TiO_2

4.2.1.2 XRD

The X-ray diffraction of Pt/0.005M-TiO_2 are shown in **Figure 4.22**, all the sample exhibited only anatase and rutile TiO_2 peaks. The peaks corresponding to transition metals doped phases were not observed, indicating that formation of nano-particle size of dopant which was not detectable by XRD or form as amorphous. The intensity of TiO_2 were decreased and appeared as broad peaks at 30° when doped transition metals due to an amorphous layer of transition metal might be covered TiO_2 surface [71]. Especially, Nb doped TiO_2 exhibited a board peak suggesting that Nb (Nb^{3+}= 86pm; Nb^{4+}= 82 pm; Nb^{5+}= 78pm) covered on TiO_2 (Ti^{4+}= 74.5pm) probably acted as an X-ray scatterer due to larger atomic radius.

4.2.1.2 H_2 temperature program reduction

The reduction behaviors of Pt/0.005Y-TiO_2, Pt/0.005La-TiO_2 and Pt/0.005Nb-TiO_2 catalysts are shown in **Figure 4.23**. Two reduction peaks were found at 50-150 ℃ and 250-450 ℃. The reduction behaviors of Pt/0.005La-TiO_2 was similar to reduction Pt/Y-TiO_2 which was discussed in 4.1.1.4. The first reduction peak was assigned to reduction Pt oxide particles [5, 73] and/or Pt-transition metal interaction. The second peak was assigned to the reduction of surface Pt-TiO_x or transition-TiO_2 interaction.

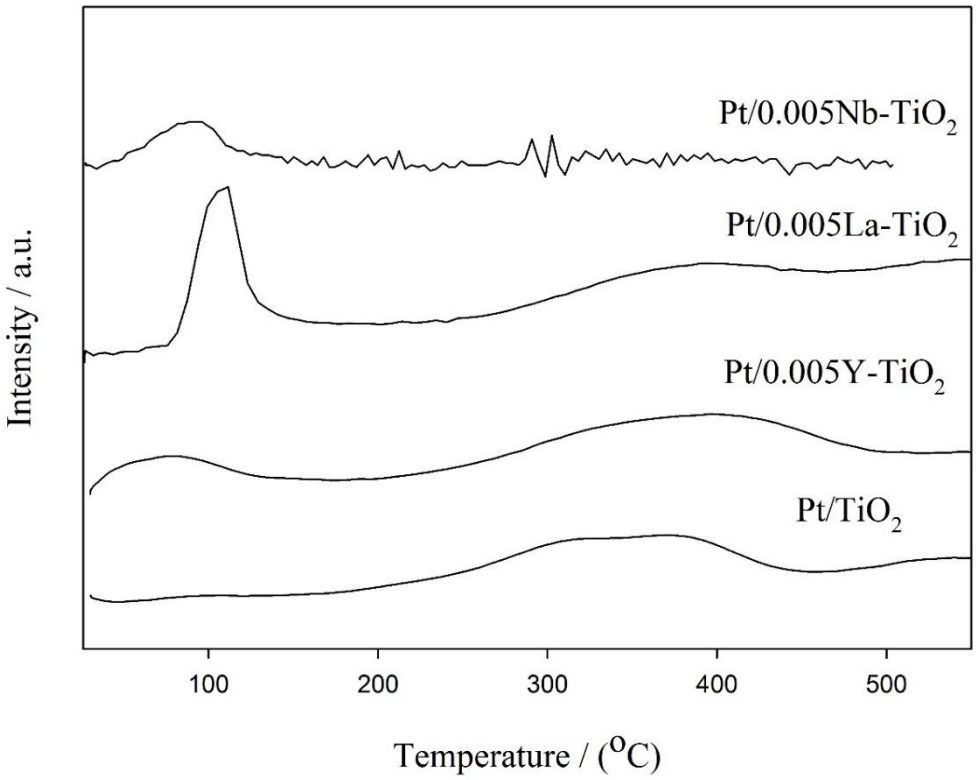

Figure 4.23 H_2-TPR of Pt/0.005Y-TiO_2 and Pt/0.005La-TiO_2 catalysts

4.2.1.4 XPS

The binding energy peaks approximately at 458.9 eV and 464.7 eV were assigned to $2p_{3/2}$ and $2p_{1/2}$ states of Ti^{4+} in TiO_2 [80], As shown in **Figure 4.24**. The binding energy shifted to higher binding energies for all transition metals doped TiO_2, especially in Pt/0.005Nb-TiO_2 which probably because of electric effect of transition, platinum and TiO_2 [89].

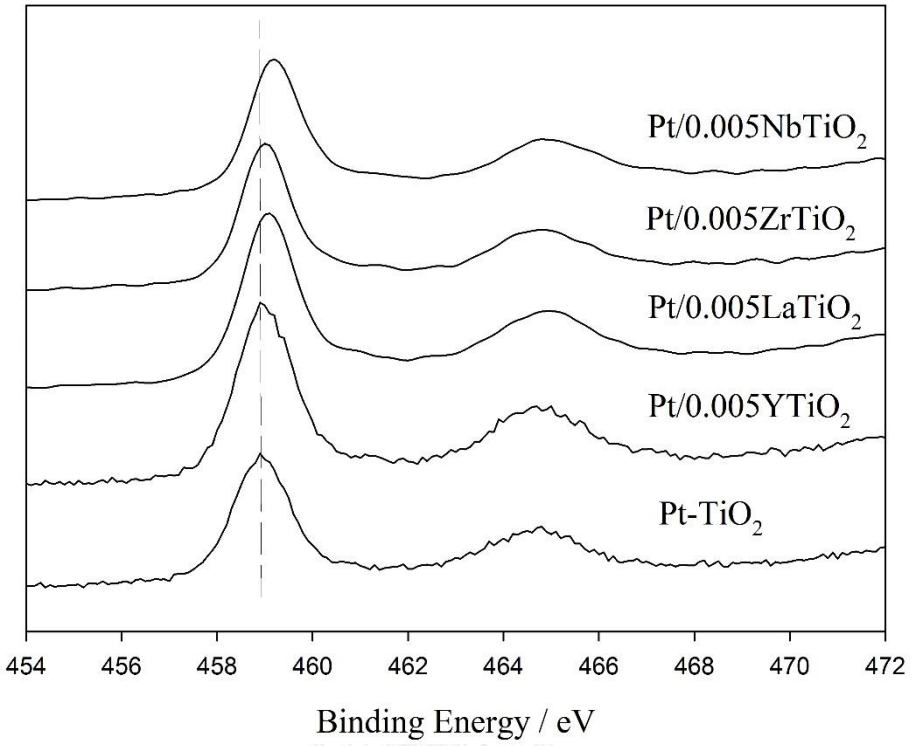

Figure 4.24 XPS spectra of Ti 2p for Pt/TiO_2 and $Pt/M\text{-}TiO_2$

4.2.1.5 Electron spin resonance (ESR)

ESR signals of trapped electrons and holds on TiO_2 and $0.005M\text{-}TiO_2$ at 130K are shown in **Figure 4.24**. the sharp signals at g = 1.975 was assigned to lattice electron trapping site (Ti^{3+}) in Degussa P25 due to rutile phase and signal at g = 1.990 was assigned to lattice electron trapping site in anatase phase [85, 86]. All dopant $0.005M\text{-}TiO_2$ exhibit Ti^{3+} higher than undoped TiO_2. The highest signal was found on the $0.005La/TiO_2$. Ti^{3+} probably correspond to atomic radius or electronegativity of dopant, which La, Y, Zr, Nb atomic radius were 195, 180, 155, 145 pm and electronegativity were 1.1, 1.22, 1.33, 1.6, respectively. The amount of Ti^{3+} decreased in the following order La > Y > Zr > Nb. However, there is no correlation observed between atomic radius and active sites (**Figure 4.21)**.

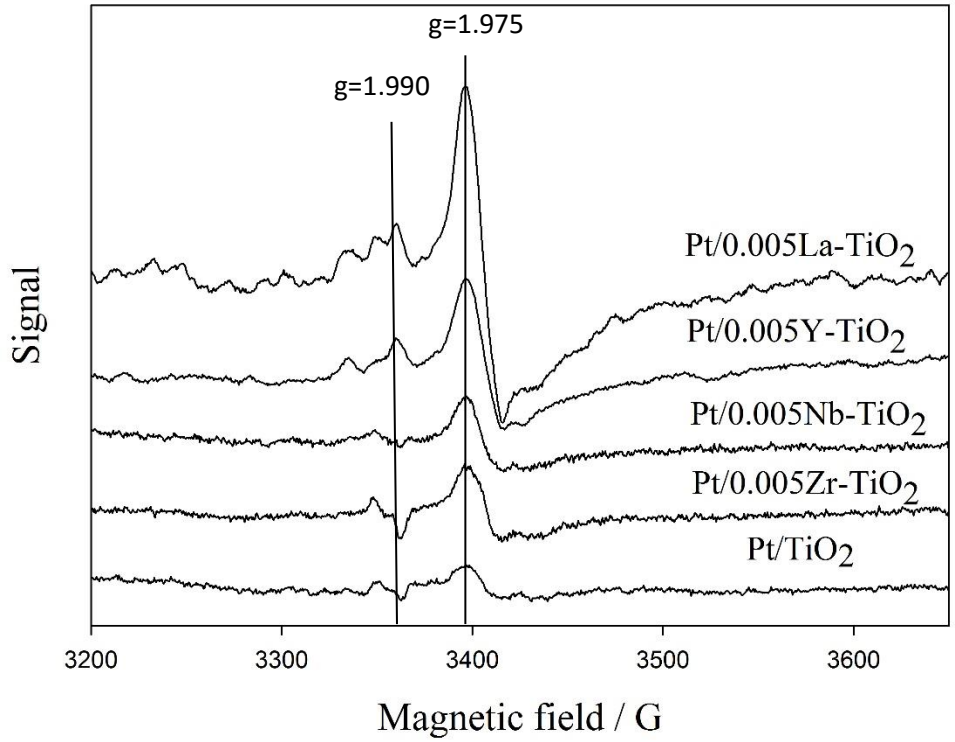

Figure 4.25 ESR spectra of Pt/0.005M-TiO_2 at 130K

4.2.1.6 Transmission electron microscope (TEM)

Figure 4.26-4.31 show the TEM image and EDX-TEM of La, Nb and Zr-TiO_2. The Pt and transition metals particle were not distinguished from TiO_2. However, the EDX-TEM indicates the presence of transition metal species similar to Pt/Y-TiO_2 results. This result indicated that highly dispersed of transition metal species on surface TiO_2 surface [22].

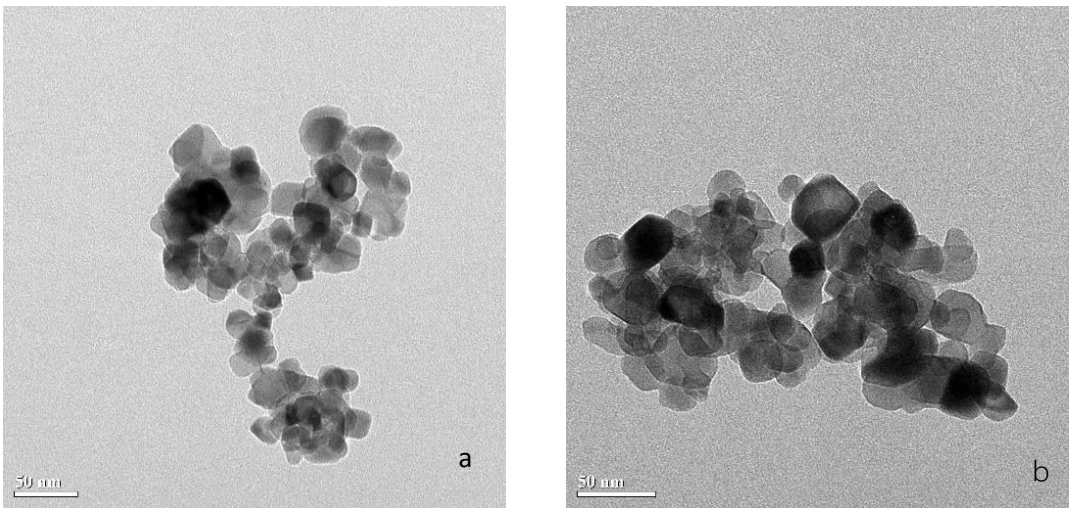

Figure 4.26 TEM image of (a) Pt/0.005La-TiO_2 and (b) Pt/0.1La-TiO_2

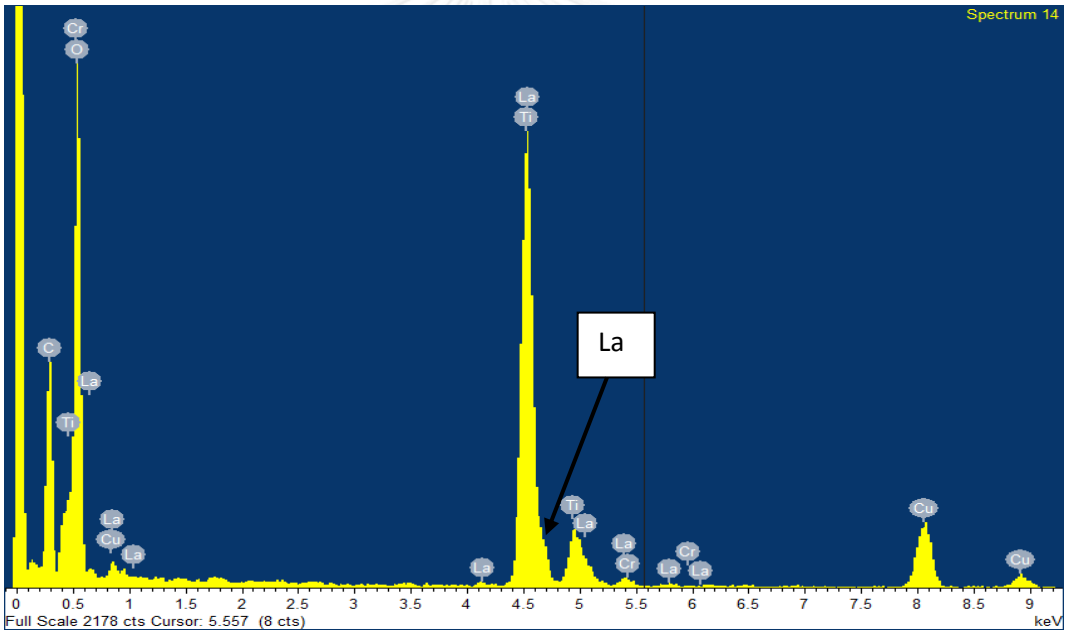

Figure 4.27 TEM-EDX analysis of Pt/0.1La-TiO_2

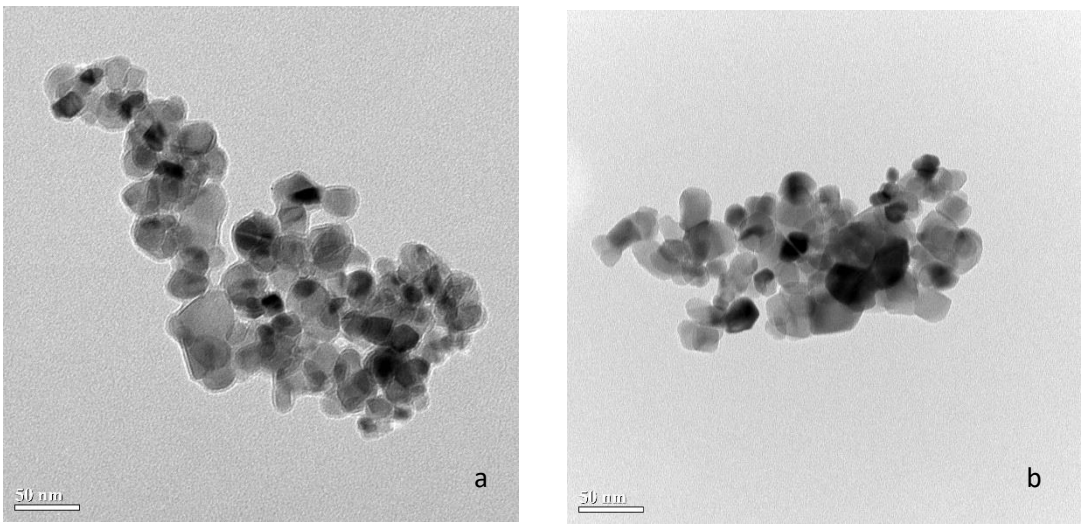

Figure 4.28 TEM image of (a) Pt/0.005Nb-TiO_2 and (b) Pt/0.1Nb-TiO_2

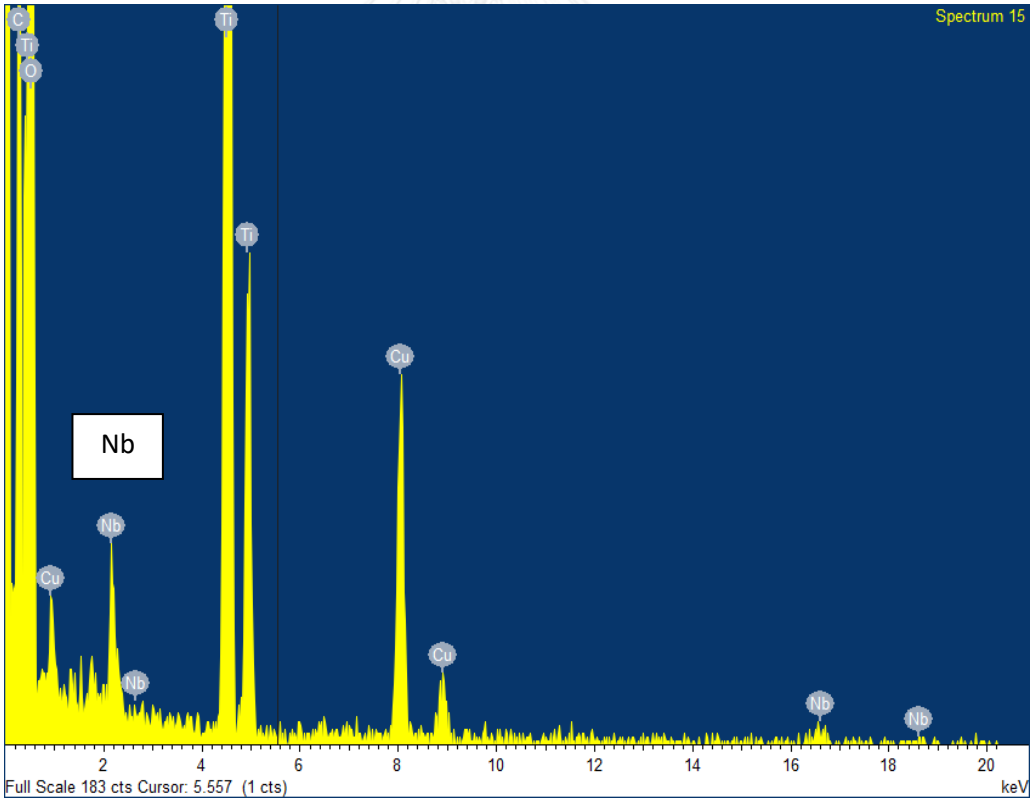

Figure 4.29 TEM-EDX analysis of Pt/0.1Nb-TiO_2

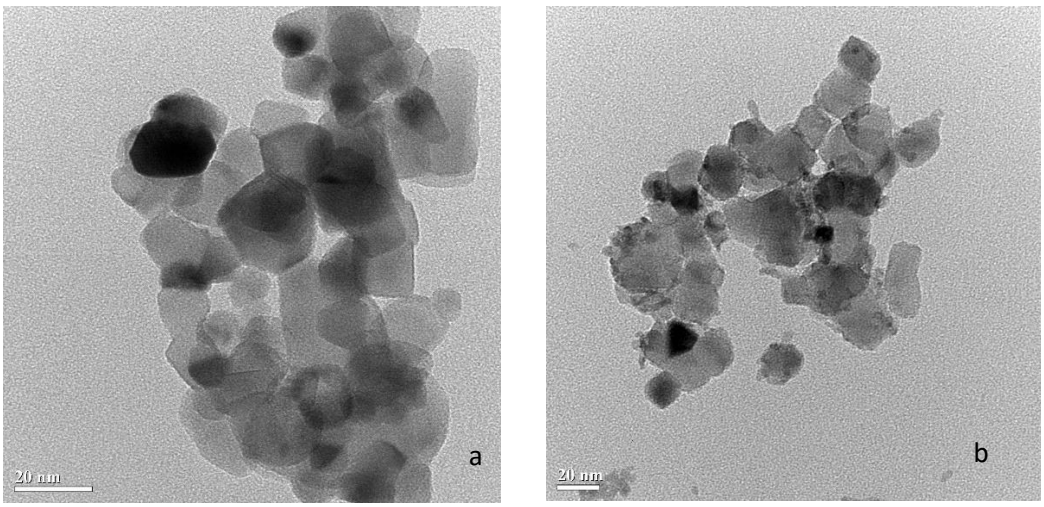

Figure 4.30 TEM image of (a) Pt/0.005Zr-TiO_2 and (b) Pt/0.1Zr-TiO_2

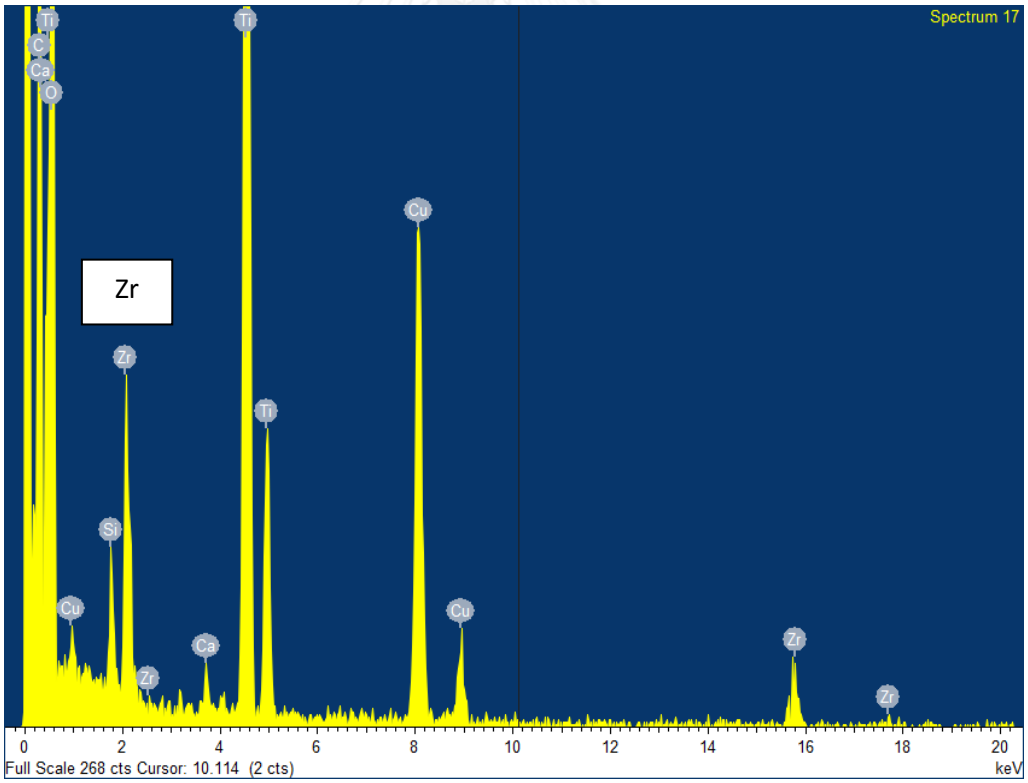

Figure 4.31 TEM-EDX analysis of Pt/0.1Zr-TiO_2

4.2.2 Effect of different dopants on the activity of CO oxidation

The catalytic activity in CO oxidation of transition metals modified TiO_2 supported Pt with various M/Ti ratios in range 0.001-0.01 are shown in **Figure 4.32-4.34**. All the transition metal doped in range 0.001-0.005 exhibited higher activity than Pt/TiO_2. The catalyst activity results showed a similar trend as in the case of active sites as shown in **Figure 4.19**. Nevertheless, the active sites of Pt/0.01M-Ti ratio was slightly different to the Pt/0.005M-TiO_2 but it exhibited lower activity than the Pt/TiO_2. A possible explanation is that higher amount of dopant may cover TiO_2 surface and Pt place on this layer, which the adsorbed CO probably not reacted with surface lattice oxygen atoms perimeter of the Pt-TiO_2 interface to generate CO_2, as discussed earlier in **section 4.1.2.**

In the case of Pt/0.005Nb-TiO_2 and Pt/0.01Zr-TiO_2, they exhibited excellent activity, a possible explanation might be influence of oxygen storage capacity of dopant. Nb_2O_5 and ZrO_2 are known as reducible support with high oxygen storage capacity [90, 91], which CO adsorbed on Pt site can react with oxygen lattice of dopant.

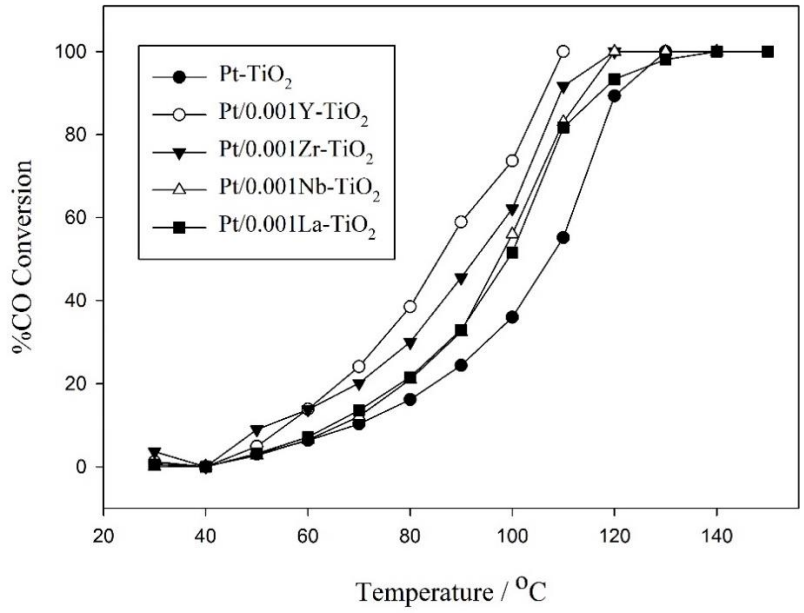

Figure 4.32 CO conversion over 0.001M/Ti of transition metals modified Pt/TiO_2

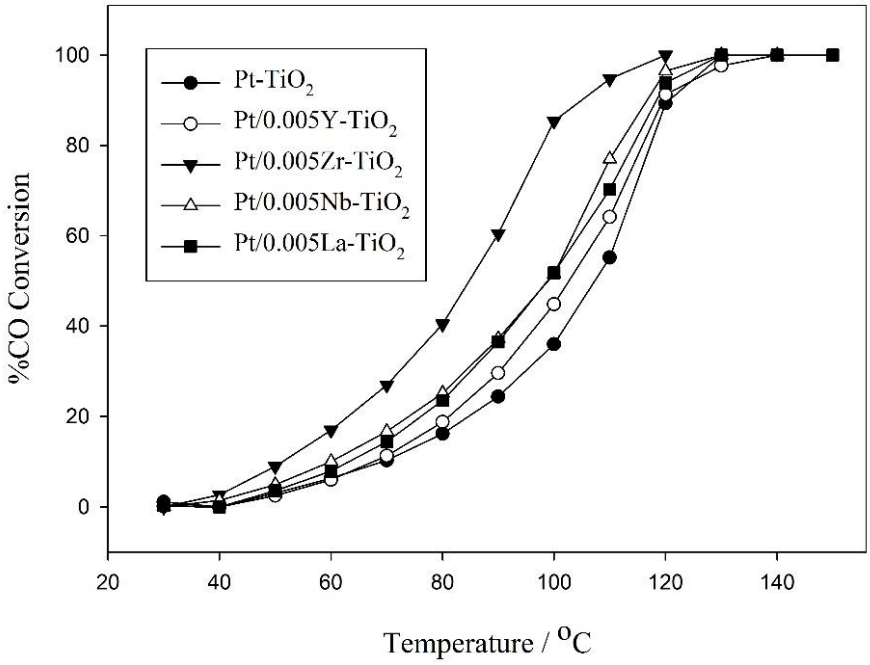

Figure 4.33 CO conversion over 0.005M/Ti of transition metals modified Pt/TiO_2

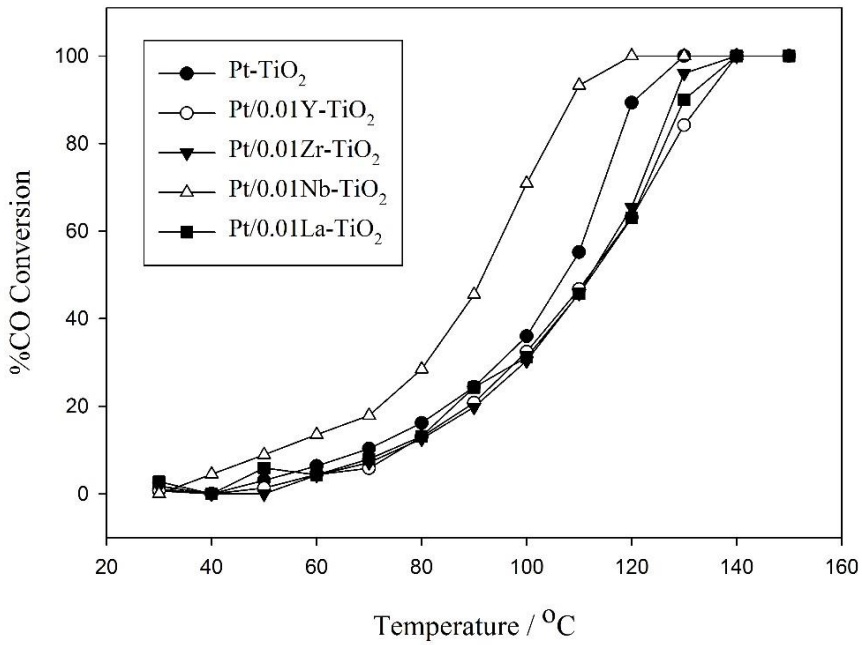

Figure 4.34 CO conversion over 0.01M/Ti of transition metals modified Pt/TiO_2

CHAPTER V
CONCULISIONS

The effect of yttria modified TiO_2 supported Pt catalysts in range 0.001-0.1 Y/Ti mole ratios was investigated. It was found that addition yttria increase Ti^{3+} on TiO_2, and led to an improvement of Pt dispersion. Pt/0.001Y-TiO_2 exhibited the highest Pt active sites and the best catalytic performance in CO oxidation. However, the active sites decreased with increasing Y/Ti ratios form 0.001 to 0.1. The excess amount of yttria probably covered TiO_2 surface and lowered Pt dispersion on this layer, which led to lower active sites (Y/Ti = 0.1). In addition, the CO adsorbed on Pt could not react with the nearly oxygen lattice on TiO_2 and led to low catalytic performance even the catalyst exhibited high amount of active sites, implying that these periphery Pt atoms were the active sites for CO oxidation.

The effect of different transition metals (La, Nb, Zr) on Pt active sites and catalytic performance was similar to the yttria modified ones. The 0.005M/Yi ratio showed the highest active sites. All dopant increase Ti^{3+} on TiO_2, the increasing of Ti^{3+} probably correspond to atomic radius or electronegativity of dopant. The transition metals doped in range 0.001-0.005 exhibited higher activity than Pt/TiO_2. Further increase of dopant than 0.005 resulted in lower activity compared to the Pt/TiO_2. Pt on dopant surface probably could not react with oxygen in TiO_2 lattice. However, Nb and Zr improve catalytic activity due to high oxygen storage and their reducible properties.

The use of transition metals modified TiO_2 as support for Pt catalysts in range 0.001-0.005 were found to be a simple method to create surface defect on TiO_2 which could lead to higher Pt active sites and catalytic activity on Pt/TiO_2.

Recommendation

1. Trend of Pt/Y-TiO_2 in range 0-0.001 Y/Ti ratio should be investigated.

2. Other transition metal ratio should be characterized

REFERENCES

[1] Mihai, O., Fathali, A., Auvray, X., and Olsson, L. DME, propane and CO: The oxidation, steam reforming and WGS over Pt/Al2O3. The effect of aging and presence of water. Applied Catalysis B: Environmental 160-161 (2014): 480-491.

[2] Hu, Y., Song, X., Jiang, S., and Wei, C. Enhanced photocatalytic activity of Pt-doped TiO2 for NOx oxidation both under UV and visible light irradiation: A synergistic effect of lattice Pt4+ and surface PtO. Chemical Engineering Journal 274 (2015): 102-112.

[3] Bailón-García, E., Carrasco-Marín, F., Pérez-Cadenas, A.F., and Maldonado-Hódar, F.J. Influence of the pretreatment conditions on the development and performance of active sites of Pt/TiO2 catalysts used for the selective citral hydrogenation. Journal of Catalysis 327 (2015): 86-95.

[4] Einaga, H., Urahama, N., Tou, A., and Teraoka, Y. CO Oxidation Over TiO2-Supported Pt–Fe Catalysts Prepared by Coimpregnation Methods. Catalysis Letters 144(10) (2014): 1653-1660.

[5] Li, N., et al. Kinetic study and the effect of particle size on low temperature CO oxidation over Pt/TiO2 catalysts. Applied Catalysis B: Environmental 142-143 (2013): 523-532.

[6] Serrano, D.P., Calleja, G., Pizarro, P., and Gálvez, P. Enhanced photocatalytic hydrogen production by improving the Pt dispersion over mesostructured TiO2. International Journal of Hydrogen Energy 39(10) (2014): 4812-4819.

[7] Comsup, N., Panpranot, J., and Praserthdam, P. Effect of TiO2 Crystallite Size on the Activity of CO Oxidation. Catalysis Letters 133(1-2) (2009): 76-83.

[8] Kim, S.S., Lee, H.H., and Hong, S.C. The effect of the morphological characteristics of TiO2 supports on the reverse water–gas shift reaction over Pt/TiO2 catalysts. Applied Catalysis B: Environmental 119-120 (2012): 100-108.

[9] Schubert, G., Gazsi, A., and Solymosi, F. Photocatalytic decomposition and oxidation of dimethyl ether over Au/TiO2. Journal of Catalysis 313 (2014): 127-134.

[10] Elsellami, L., Lachheb, H., and Houas, A. Synthesis, characterization and photocatalytic activity of Li-, Cd-, and La-doped TiO2. Materials Science in Semiconductor Processing 36 (2015): 103-114.

[11] Meksi, M., Berhault, G., Guillard, C., and Kochkar, H. Design of TiO2 nanorods and nanotubes doped with lanthanum and comparative kinetic study in the photodegradation of formic acid. Catalysis Communications 61 (2015): 107-111.

[12] Khan, M. and Cao, W. Preparation of Y-doped TiO2 by hydrothermal method and investigation of its visible light photocatalytic activity by the degradation of methylene blue. Journal of Molecular Catalysis A: Chemical 376 (2013): 71-77.

[13] Comsup, N., Panpranot, J., and Praserthdam, P. The effect of phosphorous precursor on the CO oxidation activity of P-modified TiO2 supported Ag catalysts. Catalysis Communications 11(15) (2010): 1238-1243.

[14] Tauster, S.J., Fung, S.C., and Garten, R.L. Strong metal-support interactions. Group 8 noble metals supported on titanium dioxide. Journal of the American Chemical Society 100(1) (1978): 170-175.

[15] Li, Y., et al. Strong metal-support interaction and catalytic properties of anatase and rutile supported palladium catalyst Pd/TiO2. Chemical Physics Letters 372(1-2) (2003): 160-165.

[16] Pinkaew, K., Praserthdam, P., and Jongsomjit, B. Effect of nanocrystallite size of TiO2 in Co/TiO2 and Co/TiO2-Ru catalysts on methanation. Korean Journal of Chemical Engineering 30(1) (2013): 50-54.

[17] Guo, C., Wu, Y., Wang, X., and Yang, B. Effect of the support calcination temperature on selective hydrodesulfurization of TiO2 nanotubes supported CoMo catalysts. Journal of Energy Chemistry 22(3) (2013): 517-523.

[18] Gojković, S.L., Babić, B.M., Radmilović, V.R., and Krstajić, N.V. Nb-doped TiO2 as a support of Pt and Pt–Ru anode catalyst for PEMFCs. Journal of Electroanalytical Chemistry 639(1-2) (2010): 161-166.

[19] Tapin, B., Epron, F., Especel, C., Ly, B.K., Pinel, C., and Besson, M. Influence of the Re introduction method onto Pd/TiO2 catalysts for the selective hydrogenation of succinic acid in aqueous-phase. Catalysis Today 235 (2014): 127-133.

[20] Yang, Z., Zhang, N., Cao, Y., Gong, M., Zhao, M., and Chen, Y. Effect of yttria in Pt/TiO2on sulfur resistance diesel oxidation catalysts: enhancement of low-temperature activity and stability. Catalysis Science & Technology 4(9) (2014): 3032.

[21] Cheng, X., Yuan, C., Green, N.R., and Withey, P.A. Sintering mechanisms of Yttria with different additives. Ceramics International 39(5) (2013): 4791-4799.

[22] Sakamoto, T., Kikuchi, H., Miyao, T., Yoshida, A., and Naito, S. Effect of transition metal element addition upon liquid phase reforming of methanol with water over TiO2 supported Pt catalysts. Applied Catalysis A: General 375(1) (2010): 156-162.

[23] Yin, X., He, D., Jiang, P., Zhou, G., Chen, H., and Deng, Y. Well-dispersed Pt on TiO2: A highly active and selective catalyst for hydrogenation of 3-nitroacetophenone. Applied Catalysis A: General 509 (2016): 38-44.

[24] Abdennouri, M., et al. Photocatalytic degradation of 2,4-D and 2,4-DP herbicides on Pt/TiO2 nanoparticles. Journal of Saudi Chemical Society 19(5) (2015): 485-493.

[25] Murcia, J.J., Hidalgo, M.C., Navío, J.A., Vaiano, V., Sannino, D., and Ciambelli, P. Cyclohexane photocatalytic oxidation on Pt/TiO2 catalysts. Catalysis Today 209 (2013): 164-169.

[26] Qin, X., Jing, L., Tian, G., Qu, Y., and Feng, Y. Enhanced photocatalytic activity for degrading Rhodamine B solution of commercial Degussa P25 TiO2 and its mechanisms. J Hazard Mater 172(2-3) (2009): 1168-74.

[27] Kaplan, R., Erjavec, B., Dražić, G., Grdadolnik, J., and Pintar, A. Simple synthesis of anatase/rutile/brookite TiO2 nanocomposite with superior mineralization potential for photocatalytic degradation of water pollutants. Applied Catalysis B: Environmental 181 (2016): 465-474.

[28] Nikfarjam, A. and Salehifar, N. Improvement in gas-sensing properties of TiO2 nanofiber sensor by UV irradiation. Sensors and Actuators B: Chemical 211 (2015): 146-156.

[29] Mohamad, M., Ul Haq, B., Ahmed, R., Shaari, A., Ali, N., and Hussain, R. A density functional study of structural, electronic and optical properties of titanium dioxide: Characterization of rutile, anatase and brookite polymorphs. Materials Science in Semiconductor Processing 31 (2015): 405-414.

[30] Zangeneh, H., Zinatizadeh, A.A.L., Habibi, M., Akia, M., and Hasnain Isa, M. Photocatalytic oxidation of organic dyes and pollutants in wastewater using different modified titanium dioxides: A comparative review. Journal of Industrial and Engineering Chemistry 26 (2015): 1-36.

[31] Suriye, K., Praserthdam, P., and Jongsomjit, B. Control of Ti 3+ surface defect on TiO 2 nanocrystal using various calcination atmospheres as the first step for surface defect creation and its application in photocatalysis. Applied Surface Science 253(8) (2007): 3849-3855.

[32] Liu, M., Li, H., and Wang, W. Defective TiO2 with oxygen vacancy and nanocluster modification for efficient visible light environment remediation. Catalysis Today.

[33] Linh, N.H., Nguyen, T.Q., Diño, W.A., and Kasai, H. Effect of oxygen vacancy on the adsorption of O2 on anatase TiO2(001): A DFT-based study. Surface Science 633 (2015): 38-45.

[34] Gerward, L. and Staun Olsen, J. Post-Rutile High-Pressure Phases in TiO2. Journal of Applied Crystallography 30(3) (1997): 259-264.

[35] Reyes-Coronado, D., Rodríguez-Gattorno, G., Espinosa-Pesqueira, M.E., Cab, C., Coss, R.d., and Oskam, G. Phase-pure TiO 2 nanoparticles: anatase, brookite and rutile. Nanotechnology 19(14) (2008): 145605.

[36] Arlt, T., et al. High-pressure polymorphs of anatase ${\mathrm{TiO}}_{2}$. Physical Review B 61(21) (2000): 14414-14419.

[37] Reddy, M.A., Kishore, M.S., Pralong, V., Varadaraju, U., and Raveau, B. Lithium intercalation into nanocrystalline brookite TiO2. Electrochemical and solid-state letters 10(2) (2007): A29-A31.

[38] Ohtani, B., Prieto-Mahaney, O.O., Li, D., and Abe, R. What is Degussa (Evonik) P25? Crystalline composition analysis, reconstruction from isolated pure particles and photocatalytic activity test. Journal of Photochemistry and Photobiology A: Chemistry 216(2-3) (2010): 179-182.

[39] Ohno, T., Sarukawa, K., Tokieda, K., and Matsumura, M. Morphology of a TiO2 Photocatalyst (Degussa, P-25) Consisting of Anatase and Rutile Crystalline Phases. Journal of Catalysis 203(1) (2001): 82-86.

[40] Baneshi, M., Maruyama, S., and Komiya, A. The effects of TiO2 pigmented coatings characteristics on temperature and brightness of a coated black substrate. Solar Energy 86(1) (2012): 200-207.

[41] Wang, J., He, B., and Kong, X.Z. A study on the preparation of floating photocatalyst supported by hollow TiO2 and its performance. Applied Surface Science 327 (2015): 406-412.

[42] Larumbe, S., Monge, M., and Gómez-Polo, C. Comparative study of (N, Fe) doped TiO2 photocatalysts. Applied Surface Science 327 (2015): 490-497.

[43] Ren, F., Li, H., Wang, Y., and Yang, J. Enhanced photocatalytic oxidation of propylene over V-doped TiO2 photocatalyst: Reaction mechanism between V5+ and single-electron-trapped oxygen vacancy. Applied Catalysis B: Environmental 176-177 (2015): 160-172.

[44] Sood, S., Umar, A., Mehta, S.K., and Kansal, S.K. Highly effective Fe-doped TiO(2) nanoparticles photocatalysts for visible-light driven photocatalytic degradation of toxic organic compounds. J Colloid Interface Sci 450 (2015): 213-23.

[45] Lai, C.-L., Huang, H.-L., Shen, J.-H., Wang, K.-K., and Gan, D. The formation of anatase TiO2 from TiO nanocrystals in sol–gel process. Ceramics International 41(3, Part B) (2015): 5041-5048.

[46] Liu, C., et al. Hydrothermal synthesis of N-doped TiO2 nanowires and N-doped graphene heterostructures with enhanced photocatalytic properties. Journal of Alloys and Compounds 656 (2016): 24-32.

[47] Pisduangdaw, S., Mekasuwandumrong, O., Fujita, S.-I., Arai, M., Yoshida, H., and Panpranot, J. One step synthesis of Pt–Co/TiO2 catalysts by flame spray pyrolysis for the hydrogenation of 3-nitrostyrene. Catalysis Communications 61 (2015): 11-15.

[48] Ruiz-Preciado, M.A., Kassiba, A., Gibaud, A., and Morales-Acevedo, A. Comparison of nickel titanate (NiTiO3) powders synthesized by sol–gel and solid state reaction. Materials Science in Semiconductor Processing 37 (2015): 171-178.

[49] Pazokifard, S., Farrokhpay, S., Mirabedini, M., and Esfandeh, M. Surface treatment of TiO2 nanoparticles via sol–gel method: Effect of silane type on hydrophobicity of the nanoparticles. Progress in Organic Coatings 87 (2015): 36-44.

[50] Brinker, C.J. and Scherer, G.W. Sol-Gel Science: The Physics and Chemistry of Sol-Gel Processing. Elsevier Science, 2013.

[51] Leyva-Porras, C., et al. Low-temperature synthesis and characterization of anatase TiO2 nanoparticles by an acid assisted sol–gel method. Journal of Alloys and Compounds 647 (2015): 627-636.

[52] Wang, G.Q., Lan, W., Han, G.J., Wang, Y., Su, Q., and Liu, X.Q. Effect of Nb doping on the phase transition and optical properties of sol–gel TiO2 thin films. Journal of Alloys and Compounds 509(10) (2011): 4150-4153.

[53] Plata, J.J., et al. Gold Nanoparticles on Yttrium Modified Titania: Support Properties and Catalytic Activity. Topics in Catalysis 54(1-4) (2011): 219-228.

[54] Ma, Z., Overbury, S.H., and Dai, S. Au/MxOy/TiO2 catalysts for CO oxidation: Promotional effect of main-group, transition, and rare-earth metal oxide additives. Journal of Molecular Catalysis A: Chemical 273(1-2) (2007): 186-197.

[55] Sato, Y., Terada, K., Soma, Y., Miyao, T., and Naito, S. Marked addition effect of Re upon the water gas shift reaction over TiO2 supported Pt, Pd and Ir catalysts. Catalysis Communications 7(2) (2006): 91-95.

[56] Clark, P.D., Sui, R., Dowling, N.I., Huang, M., and Lo, J.M.H. Oxidation of CO in the presence of SO2 using gold supported on La2O3/TiO2 nanofibers. Catalysis Today 207 (2013): 212-219.

[57] Hou, K.J., Meng, M., Zou, Z.Q., and Lu, Q. Effect of La3+ doping on the structures and performance of nano-structured Au/TiO2 catalysts. Chinese Journal of Inorganic Chemistry 23(9) (2007): 1538-1544.

[58] Luengnaruemitchai, A., Srihamat, K., Pojanavaraphan, C., and Wanchanthuek, R. Activity of Au/Fe2O3–TiO2 catalyst for preferential CO oxidation. International Journal of Hydrogen Energy 40(39) (2015): 13443-13455.

[59] Elezovic, N.R., Babic, B.M., Radmilovic, V.R., Vracar, L.M., and Krstajic, N.V. Nb–TiO2 supported platinum nanocatalyst for oxygen reduction reaction in alkaline solutions. Electrochimica Acta 56(25) (2011): 9020-9026.

[60] Ouyang, X. and Scott, S.L. Mechanism for CO oxidation catalyzed by Pd-substituted BaCeO3, and the local structure of the active sites. Journal of Catalysis 273(2) (2010): 83-91.

[61] Davran-Candan, T., Demir, M., and Yildirim, R. Analysis of reaction mechanisms and kinetics of preferential CO oxidation over Au/γ-Al2O3. Reaction Kinetics, Mechanisms and Catalysis 104(2) (2011): 389-398.

[62] Azar, M., et al. Insights into activation, deactivation and hydrogen-induced promotion of a Au/TiO2 reference catalyst in CO oxidation. Journal of Catalysis 239(2) (2006): 307-312.

[63] Mguig, B., Calatayud, M., and Minot, C. CO oxidation over anatase TiO2-(001). Journal of Molecular Structure: THEOCHEM 709(1-3) (2004): 73-78.

[64] Widmann, D. and Behm, R.J. Active oxygen on a Au/TiO2 catalyst: formation, stability, and CO oxidation activity. Angewandte Chemie International Edition 50(43) (2011): 10241-10245.

[65] Tanaka, K.-I., Shou, M., He, H., and Shi, X. Significant enhancement of the oxidation of CO by H2 and/or H2O on a FeO x /Pt/TiO2 catalyst. Catalysis Letters 110(3-4) (2006): 185-190.

[66] Qin, H., Qian, X., Meng, T., Lin, Y., and Ma, Z. Pt/MOx/SiO2, Pt/MOx/TiO2, and Pt/MOx/Al2O3 Catalysts for CO Oxidation. Catalysts 5(2) (2015): 606-633.

[67] Seo, P.W., Choi, H.J., Hong, S.I., and Hong, S.C. A study on the characteristics of CO oxidation at room temperature by metallic Pt. J Hazard Mater 178(1-3) (2010): 917-25.

[68] Green, R., Morrall, P., and Bowker, M. CO Spillover and Oxidation on Pt/TiO2. Catalysis Letters 98(2) (2004): 129-133.

[69] Fernandes Machado, N.R.C. and Santana, V.S. Influence of thermal treatment on the structure and photocatalytic activity of TiO2 P25. Catalysis Today 107-108 (2005): 595-601.

[70] Behnajady, M., Yavari, S., and Modirshahla, N. Investigation on adsorption capacity of TiO2-P25 nanoparticles in the removal of a mono-azo dye from aqueous solution: A comprehensive isotherm analysis. Chemical Industry and Chemical Engineering Quarterly 20(1) (2014): 97-107.

[71] Zhang, M., et al. Catalytic oxidation of NO with O2 over FeMnOx/TiO2: Effect of iron and manganese oxides loading sequences and the catalytic mechanism study. Applied Surface Science 300 (2014): 58-65.

[72] Grabowska, E., Sobczak, J.W., Gazda, M., and Zaleska, A. Surface properties and visible light activity of W-TiO2 photocatalysts prepared by surface impregnation and sol–gel method. Applied Catalysis B: Environmental 117-118 (2012): 351-359.

[73] Kim, S.S., Park, K.H., and Hong, S.C. A study of the selectivity of the reverse water–gas-shift reaction over Pt/TiO2 catalysts. Fuel Processing Technology 108 (2013): 47-54.

[74] Jabłońska, M. TPR study and catalytic performance of noble metals modified Al2O3, TiO2 and ZrO2 for low-temperature NH3-SCO. Catalysis Communications 70 (2015): 66-71.

[75] Shi, C. and Zhang, P. Effect of a second metal (Y, K, Ca, Mn or Cu) addition on the carbon dioxide reforming of methane over nanostructured palladium catalysts. Applied Catalysis B: Environmental 115-116 (2012): 190-200.

[76] Pisduangdaw, S., Mekasuwandumrong, O., Yoshida, H., Fujita, S.-I., Arai, M., and Panpranot, J. Flame-made Pt/TiO2 catalysts for the liquid-phase selective hydrogenation of 3-nitrostyrene. Applied Catalysis A: General 490 (2015): 193-200.

[77] Liu, Z., et al. Selective catalytic reduction of NOx with H2 over WO3 promoted Pt/TiO2 catalyst. Applied Catalysis B: Environmental 188 (2016): 189-197.

[78] Liu, H., Wu, H., and He, D. Methane conversion to syngas over Ni/Y2O3 catalysts — Effects of calcination temperatures of Y2O3 on physicochemical properties and catalytic performance. Fuel Processing Technology 119 (2014): 81-86.

[79] Eschemann, T.O., Oenema, J., and de Jong, K.P. Effects of noble metal promotion for Co/TiO2 Fischer-Tropsch catalysts. Catalysis Today 261 (2016): 60-66.

[80] Zhang, H., Miao, G., Ma, X., Wang, B., and Zheng, H. Enhancing the photocatalytic activity of nanocrystalline TiO2 by co-doping with fluorine and yttrium. Materials Research Bulletin 55 (2014): 26-32.

[81] Zhang, X., et al. The role of oxygen vacancy-Ti3+ states on TiO2 nanotubes' surface in dye-sensitized solar cells. Materials Letters 100 (2013): 51-53.

[82] Khan, M., Li, J., Cao, W., and Ullah, A. Advancement in the photocatalytic properties of TiO2 by vanadium and yttrium codoping: Effect of impurity concentration on the photocatalytic activity. Separation and Purification Technology 130 (2014): 15-18.

[83] Khan, M. and Cao, W. Development of photocatalyst by combined nitrogen and yttrium doping. Materials Research Bulletin 49 (2014): 21-27.

[84] Bouattour, S., Botelho do Rego, A.M., and Vieira Ferreira, L.F. Photocatalytic activity of Li+–Rb+–Y3+ doped or codoped TiO2 under sunlight irradiation. Materials Research Bulletin 45(7) (2010): 818-825.

[85] Hurum, D.C., Agrios, A.G., Gray, K.A., Rajh, T., and Thurnauer, M.C. Explaining the enhanced photocatalytic activity of Degussa P25 mixed-phase TiO2 using EPR. The Journal of Physical Chemistry B 107(19) (2003): 4545-4549.

[86] EPR investigation. The Journal of Physical Chemistry B 107(19) (2003): 4545-4549.

[87] Saqlain, M.A., Hussain, A., Siddiq, M., and Leitão, A.A. A DFT+U study of the Mars Van Krevelen mechanism of CO oxidation on Au/TiO2 catalysts. Applied Catalysis A: General 519 (2016): 27-33.

[88] Liu, H.-H., Wang, Y., Jia, A.-P., Wang, S.-Y., Luo, M.-F., and Lu, J.-Q. Oxygen vacancy promoted CO oxidation over Pt/CeO2 catalysts: A reaction at Pt–CeO2 interface. Applied Surface Science 314 (2014): 725-734.

[89] Zhao, X., et al. Highly dispersed V2O5/TiO2 modified with transition metals (Cu, Fe, Mn, Co) as efficient catalysts for the selective reduction of NO with NH3. Chinese Journal of Catalysis 36(11) (2015): 1886-1899.

[90] Chun, H.-J., Kim, D.B., Lim, D.-H., Lee, W.-D., and Lee, H.-I. A synthesis of CO-tolerant Nb2O5-promoted Pt/C catalyst for direct methanol fuel cell; its physical and electrochemical characterization. International Journal of Hydrogen Energy 35(12) (2010): 6399-6408.

[91] Mozer, T.S. and Passos, F.B. Selective CO oxidation on Cu promoted Pt/Al2O3 and Pt/Nb2O5 catalysts. International Journal of Hydrogen Energy 36(21) (2011): 13369-13378.

APPENDIX

Appendix A

Calculation for catalyst preparation

A.1 Calculation for the preparation of transition doped TiO_2 (Degussa P25)

Example calculation for the preparation of 0.001Y-TiO_2 (molar ratio of Y/Ti = 0.001)

Data for calculation: Mw. of Yttrium(III) nitrate hexahydrate = 383.01 g/mole

Mw. of TiO_2 (Degussa P25) = 79.87 g/mole

Base on 2g TiO_2 (Y/Ti ratio = 0.001)

TiO_2 2g = 0.02504 mol TiO_2 = 0.02504 mol Ti

Yttria metal required = 0.00002504 mole

Yttrium(III) nitrate hexahydrate 1mole = 1mole Y

Weight of precursor required = mole of precursor required x Mw of precursor / percent of purity

= 0.00002504 x 383.01 / 0.9999

= 0.009576 g

The 0.009576 g of Yttrium(III) nitrate hexahydrate is dissolved in 0.8 ml of de-ionized water to obtain a suitable amount of aqueous solution for 2 g of titania support

A.2 Calculation for the preparation of metal loading catalyst (0.3 wt% Pt)

Example calculation for the preparation of Pt-TiO_2

Data for calculation:

Mw. of Chloroplatinic acid hydrate ($H_2Cl_6Pt \bullet xH_2O$) = 409.81 g/mole (38% Pt basis)

Mw. of TiO_2 (Degussa P25) = 79.87 g/mole

Mw of Platinum = 195.084 g/mole

Preparation plantinum stock 20%wt/wt

1g of choloroplatanic acid hydrate was dissolved with 4ml of deionized water to design concentration stock.

Preparation 0.3wt% Pt-TiO_2 catalyst

Based on 100 g of catalyst used, the composition of the catalyst is follow;

Platinum metal (Pt) = 0.3 g

TiO_2 (Degussa P25) = 100 - 0.3 = 99.7 g

For 1 g of titania support used

Platinum metal required = 1 x (0.3/99.7) = 0.00301 g

Platinum metal 0.00301 g was acquired from $H_2Cl_6Pt \bullet xH_2O$, which has 38% of Pt basis

$H_2Cl_6Pt \bullet xH_2O$ required = 0.00301/0.38 = 0.007918 g

Thus, from the Pt stock solution with concentration 20%wt/wt

Pt stock solution required = 0.007918 x (100/20) = 0.03959 g

The 0.03959 g of Pt stock solution is dissolved in 0.4 ml of de-ionized water to obtain a suitable amount of aqueous solution for 1 g of titania support

Appendix B

CALCULATION OF CRYSTALLITE SIZE

CALCULATION OF CRYSTALLITE SIZE

The crystallite size was calculated from the width at half of height (or full- width-half-max) of diffraction peak of the XRD pattern by using the Debye-Scherrer equation.

$$D = \frac{k\lambda}{\beta \cos \theta}$$

Where D = Crystallite size, Å

K = Crystallite-shape factor or Scherrer constant depending on shape of crystal (= 0.9 for FWHM of spherical crystals with cubic symmetry)

λ = X-ray wavelength, (=1.5418 Å for CuK_α)

θ = Observed peak angle, degree

β = X-ray diffraction broadening, radian

The X-ray diffraction broadening (β) is the pure full-width-half-max of powder diffraction peak free from all broadening because of the experimental equipment or diffractometer. For a standard sample, α-Alumina is used as a standard sample to observe the instrumental broadening due to its crystallite size larger than 2000 A°. The X-ray diffraction broadening (β) can be determined by using the Warren's formula.

According to Warren's formula:

$$\beta = \sqrt{\beta_M^2 - \beta_S^2}$$

Where β_M = Measured peak width at half of peak height, radian

β_s = Corresponding full-width-half-max of the standard material (i.e., α-Alumina), radian

Example: Calculation of the crystallite size of anatase TiO_2

The major peak of anatase TiO_2 was observed at 25.48° 2θ.

Full-width-half-max of diffraction peak at 25.48° = 0.526^o

$$= \frac{2\pi \text{ x } 0.526^o}{360}$$

= 0.00918 radian

Corresponding full-width-half-max of α-alumina of diffraction peak at 25.48° = 0.00383 radian

$$\beta = \sqrt{\beta_M^2 - \beta_S^2}$$

$$= \sqrt{0.00918^2 - 0.00383^2}$$

$$= 0.00834\ radian$$

Thus, β = 0.00834 radian

2θ = 25.48° ; θ = 12.74°

λ = 1.5418 A° for CuK_α

Crystallite size, $D = \frac{k\lambda}{\beta \cos\theta}$

$$= \frac{0.9 \text{ x } 1.5418}{0.00834\ x\ \cos 12.74^o}$$

$$= \frac{k\lambda}{\beta \cos\theta}$$

= 168.52 *Å* = 16.85 nm

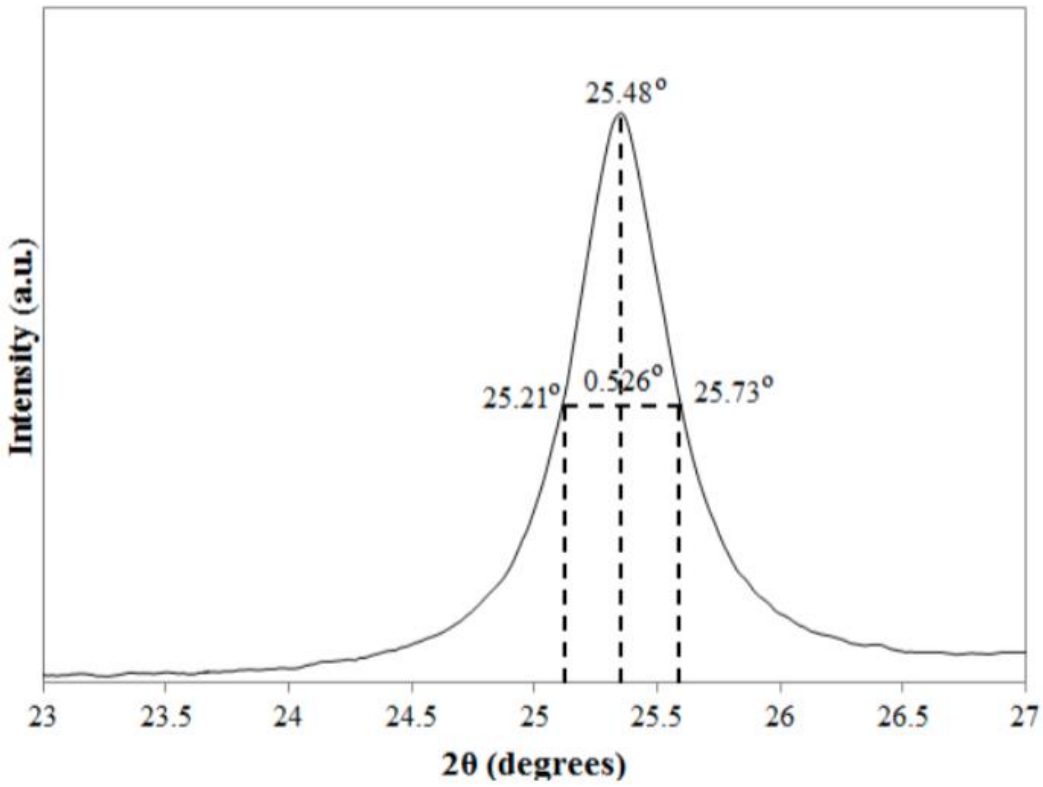

Figure B.1 The measured XRD peak of anatase TiO_2 for calculation of crystallite size of anatase TiO_2

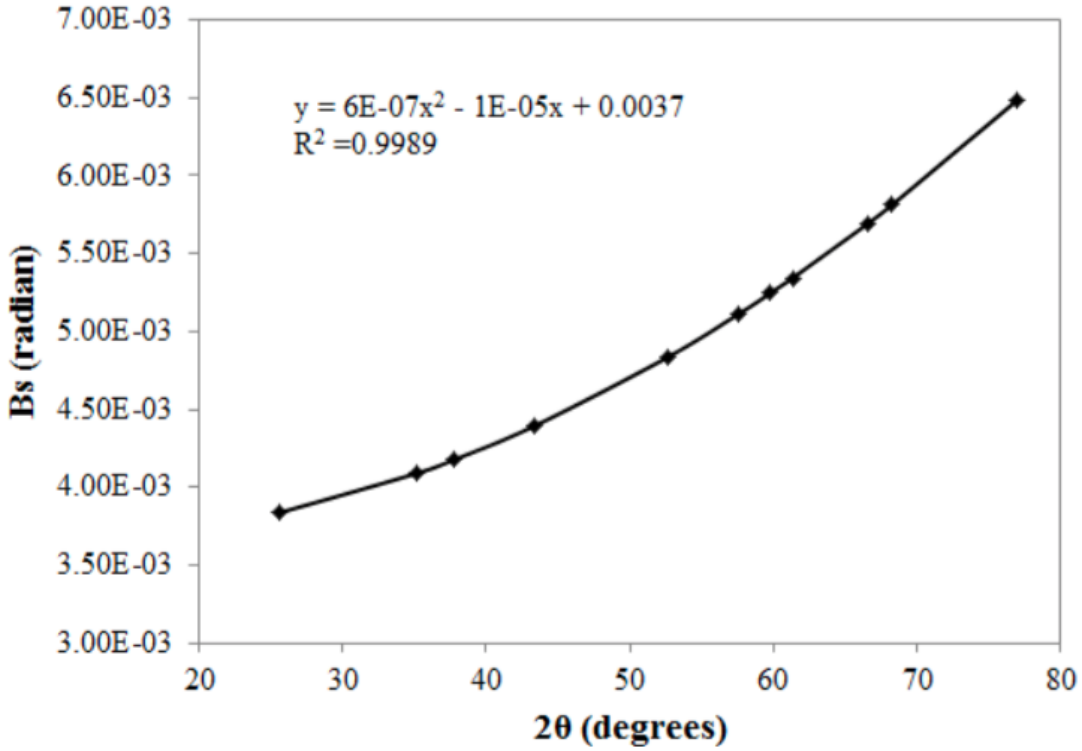

Figure B.2 The plot indicating the value of line broadening because of the equipment (data were obtained by using **α**-alumina as standard material)

Appendix C

Calculation for CO chemisorption

CO pulse chemisorption was employed to determine the metal active sites on the Pt/TiO_2

The reaction stoichiometry of CO : Pt = 1 : 1

Let

Weight of catalyst used	=	W	g
Peak area of CO per syringe	=	A	unit
Integral adsorbed area of CO	=	B	unit
Adsorbed ratio	=	B/A	unit
Adsorbed quantity per 1 syringe	=	20 x B/A	μL
Volume of CO 1mole of CO at 30°	=	24.85×10^6	μL
Mole of CO adsorbed on catalyst	=	$20 \times (B/A) / 24.85 \times 10^6$	mmol
Molecule of CO adsorbed on catalyst	=	$[20 \times (B/A) / 24.85 \times 10^6] \times 6.02 \times 10^{23}$	molecule
Molecule of CO adsorbed per g-cat.	=	$[(B/A) \times 4.845 \times 10^{23}] / W$	molecule/g-cat
Amount of metal active site	=	Molecule of CO adsorbed per g-cat.	

Example $Pt\text{-}TiO_2$

Weight of catalyst used	=	0.0560	g
Peak area of CO per syringe	=	0.03507	unit
Integral adsorbed area of CO	=	0.02084	unit
Adsorbed ratio	=	0.5942	unit
Adsorbed quantity per 1 syringe	=	11.884	μL
Volume of CO 1mole of CO at 30°	=	24.85×10^6	μL
Mole of CO adsorbed on catalyst	=	4.7823×10^{-7}	mmol
Molecule of CO adsorbed on catalyst	=	2.8789×10^{23}	molecule
Molecule of CO adsorbed per g-cat.	=	5.1408×10^{18}	molecule/g-cat
Amount of metal active site	=	5.1408×10^{18}	molecule/g-cat

VITA

Mr. Kongkitit Bungrathok was born on May 17th, 1991 in Khonkaen, Thailand. He received the Bachelor's Degree of Engineering from the Department of Chemical Engineering, Khon Kaen University 2013. After graduation, he entered study for a Master's Degree with a major in Chemical Engineering at the Department of Chemical Engineering, Faculty of Engineering, Chulalongkorn University and completed the program in 2016.